

Practical Implementation Details of Multiple Point Statistical Simulation

by

Chenyu Jiang

A thesis submitted in partial fulfillment of the requirements for the degree of

Master of Science

in

Mining Engineering

Department of Civil and Environmental Engineering
University of Alberta

© Chenyu Jiang, 2016

Abstract

Best practice and recommendations for multiple point statistics (MPS) simulation are presented. Three main contributions are: (1) assessing the stationarity of training images (TI) and determining the characteristics of TI's that result in realizations that reproduce features found in the TI; (2) determining optimal input parameters of MPS simulation; (3) summarizing categorical merging rules when implementing MPS simulation in a hierarchical MPS methodology. Specifically, the first contribution is determining what type of TI is suitable for generating MPS realizations that reproduce TI features. The quality of a TI is considered here by the quality of TI features reproduced in the MPS realizations. Stationarity is assessed through dividing a TI into zones and comparing the distribution of categories, oriental features and the Euclidean distance matrix.

Ten 2D TIs and six 3D TIs are assessed to determine the optimal input parameters to use in SNESIM. The optimal settings found depend on the dimensionality of the TI and include: using a 40-70-point template in 2D cases; 50 (or more) point templates with 3D TIs; square template shapes; and use of 4 or more multiple-grids.

Because the quality of the realizations generated with SNESIM are found to depend on the stationarity of the TI, cut-offs for determining the stationarity level of a TI is provided and is based on its statistical assessment and predicts expected realization quality.

Finally, if the TI is too complex to provide decent feature reproduction because of the number of categories, a hierarchical methodology is recommended. The TI is re-coded to a TI with fewer categories, and is simulated in multiple steps. Each simulation step is based on the results of the previous steps. Rules for combining categories are discussed: categories that share a little contact area, or are far from each other should be lumped, to

keep the isolated category separated, and lumping two categories that are completely connected.

With the popularity of MPS simulation, it is important to ensure a proper implementation of the methodology. The TIs analyzed are diverse and allow for the generalization of the findings in this thesis.

Acknowledgements

I would like to thank my supervisor Dr. Jeffery B. Boisvert for his patient guidance and support that makes this thesis possible. I would also like to thank Dr. Clayton V. Deutsch for giving the suggestions to this thesis, and for his caring for all of the students at the Centre for Computational Geostatistics.

I also want to thank my parents and my grandparents for giving me advices and respecting my decisions at all times.

Table of Content

1	Introduction	1
1.1	Problem Statement.....	1
1.2	Literature Review	2
1.3	Stationarity of the TIs	4
1.4	An Introduction to SNESIM	6
1.4.1	Theory of SNESIM.....	6
1.4.2	Multiple-grid Approach.....	9
1.5	Template Generation.....	10
1.6	MPS Assessment Approaches	12
1.6.1	Multiple Point Histogram (Clayton, 1992).....	12
1.6.2	Distribution of Runs (Mood, 1940).....	13
1.6.3	Multidimensional Scaling	14
1.7	Hierarchical Simulation	15
1.8	Thesis Outline	16
2	Stationarity of Various TIs	17
2.1	Training Images	17
2.2	Stationarity Tests	20
2.3	Methods for Assessing Stationarity	20
2.3.1	Category Distribution.....	21
2.3.2	Orientation Stationarity	23
2.3.3	MPHIST.....	25
2.3.4	Distance Matrix.....	26
2.3.5	Final Results.....	26
2.4	3D TIs Stationarity Tests	28
2.5	Discussion.....	30
3	Optimization of MPS Simulation Parameters	31
3.1	SNESIM Simulation	31
3.2	Template	31

3.3	Assessment of Geostatistical Realizations.....	37
3.3.1	The Distribution of Runs.....	38
3.3.2	Assessing Realizations using MDS.....	39
3.4	Assessing Stationarity.....	40
3.5	Discussions	42
4	Case Study of Assessing 3D TIs.....	44
4.1	Simulation of 3D TIs	44
4.1.1	SNESIM Simulation.....	44
4.1.2	Stationarity Assessment	48
4.2	Large Number of Rock Types TI Example.....	50
4.2.1	Background of the Copper TI.....	50
4.2.2	Simulation of the Large Copper TI	51
4.3	Discussions	52
5	Hierarchical Simulation.....	54
5.1	Hierarchical Simulation Methodology.....	54
5.2	Statistical Relationships for Assessing TIs	55
5.2.1	Distance between Categories.....	56
5.2.2	Contact Area.....	57
5.2.3	Transition Probability Matrix	58
5.3	Hierarchical Rule Definition.....	60
5.3.1	TIs with Three Categories.....	60
5.3.2	TIs with More Than Three Categories	63
5.4	3D TIs	69
5.4.1	3D TIs with Fewer than 6 Categories.....	69
5.5	Informed TI Patterns	75
5.6	The Large Copper TI Example	76
5.7	Discussion	79
6	Conclusions	81
6.1	Research Conclusions and Contributions	81
6.2	Recommendations.....	83
	Bibliography.....	84

Appendix A – Software	87
A.1 Introduction.....	87
A.2 Updated SNESIM Program	87
A.3 Created Statistical Relationship Calculation Program.....	88
A.3.1 Distance	88
A.3.2 Contact Area.....	89
Appendix B – Workflow for Lumping in Hierarchical Approach.....	89

List of Figures

1.1	Examples of stationary TIs (a), (b), and non-stationary TIs (c), (d).....	6
1.2	A simulated value is drawn by generating a uniform random number in (0, 1) and reading for the quantile	8
1.3	A grid of size 8×8 cells using three nested increasingly finer grids of a multiple-grid simulation sequence	9
1.4	Intermediate grid adding within the previous simulated cells	10
1.5	Four examples of entropy-based templates for TIs	11
1.6	An example of a four-point configuration with 2 categories, generating 16 classes of combinations and is scanned over a TI.....	12
2.1	2D TIs	18
2.2	3D TIs	19
2.3	An example of decomposing a 2D TI into 9 sub-regions	21
2.4	An example of merging categories	21
2.5	An example of category histograms for subsections of TI with 3 rock types....	23
2.6	PDF of von Mises distribution.....	24
3.1	Eight examples of entropy-based templates	32
3.2	3D surface plot of the size of the template, the number multi-grids, and Δ MPHIST	33
3.3	Δ MPHIST results for 10 templates with 4 and 5 multi-grids	34
3.4	Realizations using different numbers of multi-grids	35
3.5	Eight examples of square- and rectangular-shaped templates	35
3.6	Δ MPHIST of two types of templates	36
3.7	Results of the distribution of runs for 10 TIs using different templates	38
4.1	Six 3D TIs	45
4.2	Comparing Δ MPHIST of 10 different template sizes.....	45
4.3	Δ MPHIST for three-data spacing and unconditional realizations	48
4.4	Porphyry model and drillings for conditional simulation	51
5.1	Some lumpings of the porphyry TI.....	54

5.2	An example of the shortest distance between two categories A 5-category TI	56
5.3	A 5-category TI.....	57
5.4	An example of contact relationship	58
5.5	An example of transition probability computation	59
5.6	TIs with only 3 categories.....	60
5.7	Testing Δ MPHIST results of all 6 possible orderings	61
5.8	Comparing Δ MPHIST of realizations from 18 orderings for the porphyry TI in hierarchical simulations to the traditional simulation that simulates all categories simultaneously	64
5.9	Examples of merged patterns in every step (arrow indicates the sequence	66
5.10	Comparing Δ MPHIST of realizations from 100 orderings in hierarchical simulations to the traditional simulation that simulates all categories at the same time	67
5.11	3D TIs	69
5.12	Comparing Δ MPHIST results for hierarchical simulation results to traditional simulation results	71
5.13	Comparing Δ MPHIST results for hierarchical simulation results to traditional simulation results	73
5.14	Δ MPHIST plot of the TI4	74
5.15	Slices of the TI.....	77
5.16	Six slices of hierarchical simulation	78
5.17	Realizations of standard MPS simulation	79
B.1	The binary TI in the first step.....	90
B.2	The TI in the second step	90
B.3	The TI in the third step.....	90
B.4	The TI in the fourth step.....	91
B.5	The TI in the first step	91
B.6	The TI in the second step	91
B.7	The TI in the third step.....	91
B.8	The TI in the first step.....	92
B.9	The TI in the second step	92

B.10	The demonstration of cookie-cut realizations and re-coding to final realization	
	93

List of Tables

2.1 (a)	Stationarity calculation results for four methods.....	27
2.1 (b)	Stationarity calculation results for four methods	28
2.2	Stationarity test results for 3D TIs	29
3.1	Δ MPHIST in multidimensional space scatter plots and realizations comparison.....	39
3.2 (a)	An assessment of TI stationarity	40
3.2 (b)	An assessment of TI stationarity	41
3.3	Cut-offs for stationarity level.....	42
4.1 (a)	Conditional realizations with different data spacing and unconditional realizations	46
4.1 (b)	Conditional realizations with different data spacing and unconditional realizations	47
4.2	Evaluate stationarity by statistics and unconditional simulation performance	49
4.3	Cut-offs for stationarity level.....	50
4.4	Conditional realizations with three data spacing and unconditional realizations	52
5.1	Distance between pairs of categories	57
5.2	Contact area for pairs of categories	58
5.3	Transition probability for paris of categories.....	59
5.4	The minimum and maximum Δ MPHIST realizations for different orderings...	62
5.5	Contact area (red is not so related, green is closely related).....	63
5.6	Distance between categories	63
5.7	Transition probability matrix	63
5.8	Realizations.....	65
5.9	Comparing realizations of hierarchical simulation and traditional simulation ..	68
5.10	Statistical relationships for TI2 (green means closely related, red means not so close)	70
5.11	Statistical relationships for TI3 carbonate	70
5.12	Statistical relationships for TI4 fluvial-deltaic	70

5.13	Comparing realizations of hierarchical simulation and traditional simulation..	72
5.14	Comparing realizations of hierarchical simulation and traditional simulation..	73
5.15	Comparing realizations of hierarchical simulation and traditional simulation..	75
5.16	Comparing the best ordering in informed patterns method to Δ MPHIST results; the value in fourth column is the location of the best ordering found in “# of informed patterns” test in Δ MPHIST test	76

List of Symbols

Symbol	Definition	First use
S	variable.....	1
K	possible states	1
$P(Z(s))$	probability of random variables	4
$E(Z(s))$	mean of random variables	4
$Cov(Z(s+\mathbf{h}), Z(s))$	covariance between $Z(s+\mathbf{h})$ and $Z(s)$	4
$Var(Z(s+\mathbf{h})-Z(s))$	variance between $Z(s+\mathbf{h})$ and $Z(s)$	4
$\gamma(\mathbf{h})$	variogram of lag distance \mathbf{h}	4
s_k	one state.....	6
k	one possible state.....	6
d_n	a data event	6
n	lag vectors around the central location	6
\mathbf{u}	un-sampled location.....	6
\mathbf{h}_α	geometry template	6
α	data value.....	6
$S(\mathbf{u})$	random variable.....	7
A_k	indicator random variable associated to the appearance of state	7
D	binary random variable associated to the appearance of data event.....	7
\forall	for all	8
$c\{d_n\}$	the number replicates of the conditioning data event	8
$c_k\{d_n\}$	the number replicates based previous data event.....	8
g	the level of multiple-grid	9
H_n	a two-point entropy of an n -point MPS template	10
$P_{kk'}$	the probability of categories k occurring at the central point and categories k' occurring at point n of the template	10
f_i^{Real}	the frequency corresponding to bin i for the realization	11

f_i^{TI}	the frequency corresponding to bin i for the TI.....	11
$diff$	difference between the realizations to the TI.....	11
L	a run of length	11
z_k	a sequence of $L+2$ adjacent nodes	11
f_l^1	the cumulative frequency of realization for runs length of l	12
f_l^2	the cumulative frequency of TI for runs length l a run of length	12
pat_T^m, pat_T^n	patterns from the image	13
Z_i	sub-regions chosen from the TI.....	19
$H_i(k), H_j(k)$	normalized categorical histogram	21
$D(i, j)$	difference between two histograms.....	21
α	the major direction of features	22
θ	the mean direction of the distribution between $[0, 2\pi]$	22
κ	the concentration parameter	22
α_{ti}	confidence level of the TI.....	23
δ_{uv}	difference between pattern u and v	24
d_{ij}	distance counted between categories i and j	54
E_i	ellipses are used to demonstrate categorical relationship.....	54
A_i	area of the ellipses	55
C	the border of contacting categories	55
t_{ij}	the probability of transiting category i to category j	56
$T(\mathbf{h})$	the transition probabilities matrix.....	57

List of Abbreviations

MPS	Multiple point statistics.....	1
TI	Training image	1
SNESIM	Single Normal Equation simulation	2
MPHIST	Multiple point histogram	11
MDS	Multidimensional scaling	13

Chapter 1

Introduction

1.1 Problem Statement

Geostatistics is the application of the formalism of random functions to the exploration and estimation of natural phenomena (Matheron, 1962). Geostatistics has gained popularity as a quantitative tool to generate multiple geological models that honor various types of measured and interpreted data. Conventional geostatistical techniques use the variogram and cannot capture curvilinear features or high order complex structures that appear in reservoirs (Strebelle, Conditional Simulation of Multiple Point Statistics, 2002). Multiple Point Statistics have been proposed to improve the efficiency and predictability of models compared to simultaneous approaches. Multiple Point Statistics, abbreviated as MPS, capture high-order statistics from a conceptual training image (TI). In this thesis, the following questions are addressed: (1) What type of TI is proper for MPS simulation? (2) How to choose input parameters in MPS simulation? (3) How to assess the behavior of simulation through comparing multiple realizations? (4) How to improve simulation results? Determination on practical implementation of MPS simulation is answered in this thesis, specifically:

Thesis statement: *The use of appropriate MPS simulation settings with a high quality TI improves reproduction of geological features in MPS realizations.*

1.2 Literature Review

Over the last 20 years, MPS modeling has been widely used in numerous fields. In contrast to conventional variogram-based simulation, MPS simulation extracts and reproduces multiple-point moments from a TI. The TI is a numerical conceptual representation that quantifies geological heterogeneity relevant for the reservoir of deposit (Caers, 2002). A TI should have the correct proportions of each rock type or category. It is not necessary to be the same size as the realization being simulated, but it should be big enough to represent all categories and permit calculation of conditional probabilities for a reasonable number of configurations (Deutsch and Pyrcz, 2014).

Guardiano and Srivastava (1993) proposed the use of a conceptual geological model to capture multiple point statistics by scanning a TI instead of modeling a variogram. One of the first MPS simulation programs named ENESIM was based on the principle of Sequential Indicator Simulation. It estimates the local conditional distribution by scanning the whole TI repetitively looking for patterns that match the local conditioning data, hence this program suffered from CPU expense. Strebelle (2002) then introduced an efficient dynamic search tree to store the MPS. The main advantage is search tree structure where multiple point probabilities can be retrieved directly during the simulation. In addition to the search tree, Strebelle also implemented a multiple-grid approach that is used to capture large-scale structure while considering a reasonably small template.

The Single Normal Equation algorithm was introduced by Strebelle (2002) for applying MPS simulation, which has been widely implemented in MPS simulations, but there is little guidance on selecting parameters. Liu (2006) explained and had sensitivity tests for tens of important parameters in SNESIM by using a single channel TI. Liu compared realizations

the results of changing the parameter settings including the target proportions, number of multiple-grids, and different shapes of the search neighborhood. However, while these parameters may be appropriate for that one TI, parameters may be TI specific. Many reports agree with the importance of the template shape or size in the SNESIM approach. There is little guidance on how to decide choose a template. Silva (2014) gave detailed instructions on the SNEISM program. He suggested that the “maximum conditioning data,” affects the size of the template, which is sensitive to a small value, but there was no definite answer presented how to choose specific value. Goodfellow et al., etc. (2012) suggested to increase the amount of points in the application of the template, which is also a common way to improve the reproduction of patterns in the realization. Rezaee et al., etc. (2014) suggested a template size of 160 points for a 3D model. Hashemi et al., etc. (2014) used three multiple multiple-grids to reasonably increase the search distance of the template with a small number of grid nodes. To guarantee the connectivity of simulated channel bodies, they also used a template that was elongated toward the direction of the channels. The optimal parameter settings of SNESIM are discussed in this thesis.

New approaches using MPS information have emerged. Two main research avenues have been developed. The first one is simulating patterns instead of individual pixels. A pattern-based approach, FILTERSIM, proposed by Zhang et al., (2006) introduces an idea of filters to group high dimensional patterns by a smaller set of filter scores. A training pattern from a prototype class closest to the local conditioning data event can be pasted in the simulation grid. Another pattern-based algorithm SIMPAT, presented by Arpat and Caers (2007), aims at generating realizations that reproduce the multiple-scale patterns on the simulation grid.

There are alternative search tree implementations. Comunian et al., (2011) replaced search trees with allocated lists called IMPALA. Zhang and et al., (2012) proposed a memory-efficient compact search tree algorithm. Renard and Mariethoz (2014) listed several new achievements in theory and implementation details to improve MPS based simulation. Straubhaar, Walgenwitz and Renard (2013) presented a new parallel list structure. Tan, Tahmasebi and Cares (2014) compared several TI based algorithms using a measure of distance between the realizations.

1.3 Stationarity of the TIs

Stationarity in conventional geostatistics can be defined as the decision of how to pool data together for subsequent analysis (Wilde, 2011). Stationarity is quantified by “strong”, “weak”, and “intrinsic”. “Assume that the mean $E(Z(s)) = \mu$ and the variance of $Z(s)$ exists. Strong (strict) stationarity is that the joint probability distribution of the data depends only on the relative positions of the sites at which the data were taken. The joint distribution has the following property:

$$\begin{aligned} P(Z(s_1) \leq z_1, Z(s_2) \leq z_2, \dots, Z(s_n) \leq z_n) \\ = P(Z(s_1 + \mathbf{h}) \leq z_1, Z(s_2 + \mathbf{h}) \leq z_2, \dots, Z(s_n + \mathbf{h}) \leq z_n) \end{aligned} \quad \text{Equation 1.1}$$

The property of weak (second-order) stationarity is that: the mean is constant $E(Z(s)) = \mu$; the covariance for all s is dependent only on distance $Cov(Z(s + \mathbf{h}), Z(s)) = C(\mathbf{h})$.

$$\text{At } \mathbf{h}=0: Cov(Z(s + 0), Z(s)) = C(0) = Var(Z(s)) \quad \text{Equation 1.2}$$

Intrinsic stationarity is the more general, which has the property:

1. when the difference $E(Z(s + \mathbf{h})) - Z(s)$ is second order stationary:

$$E(Z(s + \mathbf{h})) - Z(s) = 0 \quad \text{Equation 1.3}$$

$$\text{then } Var[Z(s + \mathbf{h}) - Z(s)] = 2\gamma(s + \mathbf{h} - s) = 2\gamma(\mathbf{h}) \quad \text{Equation 1.4}$$

2. second order stationarity implies intrinsic stationarity but the reverse is not implied;
3. note the similarity between intrinsic stationarity and second order stationarity: intrinsic is defined in terms of the variogram and second order is defined in terms of the covariance function;
4. the variogram is a generalization of the covariance function and under second order stationarity the two functions are related.” (Spatial Statistics, University of Southern California, course PM599, 2013)

In this thesis, “stationarity” only accounts for the quality of a TI, which should have repetitive and constant patterns to be representative of the relevant geological site being modeled, and to generate high quality realizations with accurate feature reproductions. MPS simulation relies on the availability of a stationary TI because the quality of a TI influences directly on the quality of the realizations. Strong stationarity is the foundation of accurate and representative realizations of the study area.

Strebelle and Zhang (2005) proposed a series of rotation transforms to allow non-stationary features. Mirowski et al., (2009) presented a number of methods to quantify the validity of TI by providing scale estimation, orientation and category distribution stationarity scores. Silva and Deutsch (2014) presented an interpretation of strong and weak stationarity for TIs. “Strong stationarity is the spatial configuration remains the same despite the data location. The weaker stationarity assumption in distinct regions of deposits may be confirmed by computing how the expected value and variance change over the domain”. Several stationary assessment approaches including stationarity scores on different types of TIs are implemented in Chapter 2. A geologic domain is commonly non-stationary; nevertheless, it is widely accepted that the TI used in MPS simulation should be

stationary. Figure 1.1 show two types of TIs that are stationary and non-stationary. The first two images do not show large scale trends while the last two show distinct trends and large scale global changes.

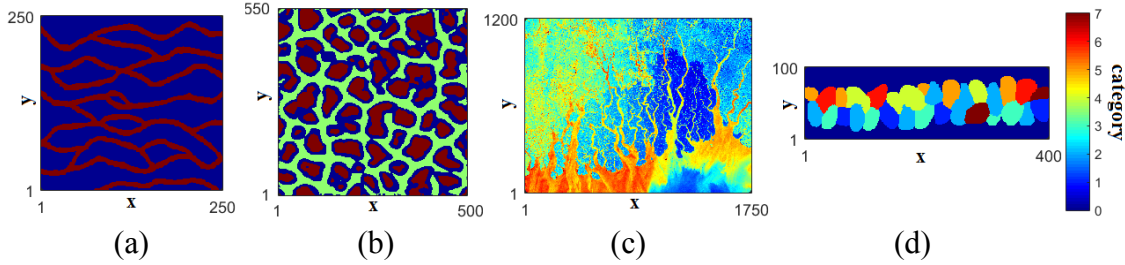


Figure 1.1: Examples of stationary TIs (a), (b), and non-stationary TIs (c), (d).

1.4 An Introduction to SNESIM

1.4.1 Theory of SNESIM

The SNESIM program is an original and important public domain software that is widely used for MPS simulation. The strength of SNESIM lies in its simple but rigorous methodology of combining the conventional sequential simulation paradigm with the search tree concept for storing probabilities derived from a TI and effectively use of the multiple-grid approach (Tran, 1994). The basic theory of the single normal equation algorithm is described as follow:

Consider a random variable S taking K possible states $\{s_k, k=1, \dots, K\}$. A data event d_n of size n being centered at an un-sampled location \mathbf{u} is defined as:

- The data location geometry defined by n vectors $\{\mathbf{h}_\alpha, \alpha=1, \dots, n\}$ relative to a central position at “0”
- The n data values defined by $\{s(\mathbf{u}+\mathbf{h}_\alpha), \alpha=1, \dots, n\}$

A data template is an n -lag vector, constituted by the previous data geometry. The value at the centre of data template is unknown as $s(\mathbf{u})$. The data event d_n is the conditioning data event constituted by n data values at the template locations.

The K possibilities of random variable $S(\mathbf{u})$ are characterized by their conditional probability distribution function:

$$\text{Prob}\{S(\mathbf{u}) = s_k | d_n\} = f(\mathbf{u}; k | d_n), k = 1, \dots, K \quad \text{Equation 1.5}$$

Jointly considering the n data event d_n , $(n+1)$ -point covariance are required to measure the dependence of $S(\mathbf{u})$ on the data event d_n . Let A_k be the indicator random variable associated to the appearance of state s_k at location \mathbf{u} , which is denoted as:

$$A_k = \begin{cases} 1 & \text{if } S(\mathbf{u}) = s_k \\ 0 & \text{otherwise} \end{cases} \quad \text{Equation 1.6}$$

Let D be the binary random variable associated to the appearance of data event d_n constituted by the n conditioning data $S(\mathbf{u}_\alpha) = s_{k_\alpha}, \alpha = 1, \dots, n$:

$$D = \begin{cases} 1 & \text{if } S(\mathbf{u}_\alpha) = s_{k_\alpha}, \forall \alpha = 1, \dots, n \\ 0 & \text{otherwise} \end{cases} \quad \text{Equation 1.7}$$

The conditional probability of $(n+1)$ -point relevant to A_k and its data event D follows Bayes Law:

$$\text{Prob}\{A_k = 1 | D = 1\} = \frac{\text{Prob}\{A_k = 1, D = 1\}}{\text{Prob}\{D = 1\}} \quad \text{Equation 1.8}$$

The denominator probability of $\{S(\mathbf{u}_\alpha) = s_{k_\alpha}, \alpha = 1, \dots, n\}$ can be inferred by counting the number $c(d_n)$ of replicates of the conditioning data event $d_n = \{S(\mathbf{u}_\alpha) = s_{k_\alpha}, \alpha = 1, \dots, n\}$ in the TI. A replicate should be the same geometric configuration and the same data values. While the numerator $\{S(\mathbf{u}) = s_k, S(\mathbf{u}_\alpha) = s_{k_\alpha}, \alpha = 1, \dots, n\}$ are inferred by counting the number $c_k\{d_n\}$ of replicates, among the previous $c\{d_n\}$, associated to a central value $S(\mathbf{u})$ equals to $s(k)$.

Thus, the conditional probabilities are calculated directly from the TI without the need to model a variogram. The required conditional probability is then identified to the training proportion $\frac{c_k(d_n)}{c(d_n)}$:

$$P(\mathbf{u}; s_k | (n)) = Prob\{A_k = 1 | D = 1\} = Prob\{S(\mathbf{u}) = s_k | (n)\} = \frac{c_k(d_n)}{c(d_n)} \quad \text{Equation 1.9}$$

The simulation grid is visited sequentially in a random path. Once a node is simulated, the value will become a hard datum that conditions the simulation of the nodes visited later in the sequence. Following is the workflow of SNESIM program:

- (1) Visit an un-sampled node \mathbf{u} ;
- (2) Search for n conditioning data and previously simulated locations;
- (3) Scan the TI (or check the search tree) for all replicates d_n and calculate the frequency of having each categories k ;
- (4) Draw a value from the categorical cdf built in the previous step;
- (5) Go back until all locations are informed.

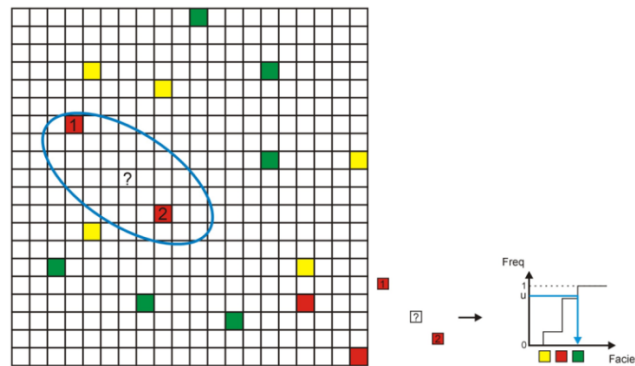


Figure 1.2: A simulated value is drawn by generating a uniform random number in (0, 1) and reading for the quantile (Unpublished CCG course, 2008)

1.4.2 Multiple-grid Approach

Multiple-grid, or multi-grid, is presented to capture the large scale structure in a TI by simulating from coarse grids to finer grids (Strebelle, 2002). There is an example of size 8×8 cells using three nested increasingly finer grids of a multi-grid simulation sequence (Strebelle, 2014) given in Figure 1.3. White cells are un-visited locations in the previous step; black cells are locations that are already simulated, and grey cells are locations being simulated at the current step. The g -th grid is constituted by every 2^{g-1} th node of the final simulation grid. The data template is therefore re-scaled proportionally to the spacing of the nodes in the grid being simulated, in order to capture the large-scale structures at the coarse grid using a same size of the template which captures small-scale structures at the finer grid. The number of multi-grids and the changes to the resulting realizations are discussed in detail in Chapter 3.

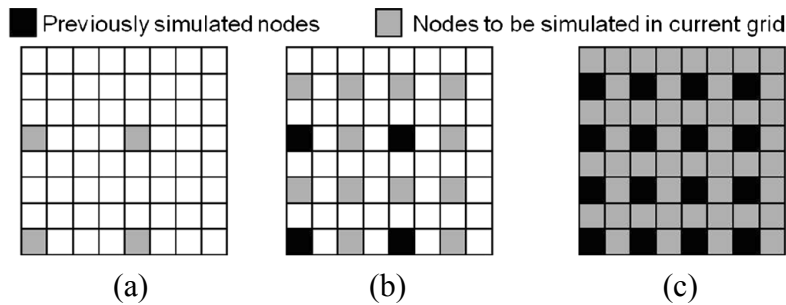


Figure 1.3: A grid of size 8×8 cells using three nested increasingly finer grids of a multiple-grid simulation sequence (Strebelle, 2012): (a) 4 simulated nodes (grey), while white cells are not visited; (b) 12 new nodes are simulated while 4 previously simulated (black) are frozen; (c) repeating process (b).

Strebelle and Cavelius (2014) proposed a memory-saving multi-grid approach. Based on the original multi-grid approach, the new method introduces intermediate multi-grids in the original multiple-grid approach, (Figure 1.4), in order to improve the speed of SNESIM. The introduction of intermediate multi-grids increases the percentage of previously simulated node and therefore reduces the size of search data template. All of simulation is based on the original SNESIM, this method will no longer discussed in this thesis.

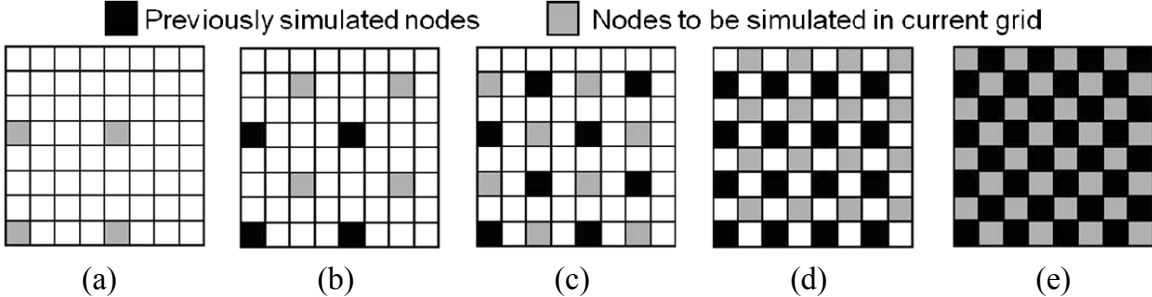


Figure 1.4: Intermediate grid adding within the precious simulated cells (Strebelle, 2012): (a) 4 nodes are simulated, white cells are not visited; (b) 4 nodes in (a) are frozen (black), and 4 intermediate nodes simulated (grey); (c), (d) and (e) repeating the process of (b).

1.5 Template Generation

The template is an important parameter that has been discussed in many MPS-related reports. With the purpose of capturing all information from a TI, a template should not be too small to overlook the whole pattern, but also cannot be too large with few replicates and large memory requirements. The greater the variety of features in a template, the more difficult it to search and the resulting probabilities may be unstable. The data search template adapted for the various nested simulation grids need not have the same geometric configuration. There is little guidance on creating or deciding on the template. One template creation method was presented by Lyster (2006). The method is an entropy-based approach of establishing the template to decide the arrangements of points used in a

template, while minimizing the memory at the same time. A two-point entropy of an n -point MPS template is defines as:

$$H_n = -\sum_{k=1}^K \sum_{k'=1}^K P_{kk'} \cdot \ln(P_{kk'}) \quad \text{Equation 1.10}$$

In Equation 1.6, K is the number of possible categories, $P_{kk'}$ is the probability of categories k occurring at the central point and categories k' occurring at point n of the template. Higher entropy indicates more randomness, which leads to less correlation between central and estimated point. Therefore, the points with lowest entropy should be considered in the template. Figure 1.5 show four examples of TIs and their corresponding entropy templates. Entropy increases from the centre to the outside, so the effective template is chosen from the central location. Chapter 3 will compare the simulation results by using the entropy-based template to the same size of regular shaped template; Chapter 4 and Chapter 5 will implement the entropy-based template in simulation.

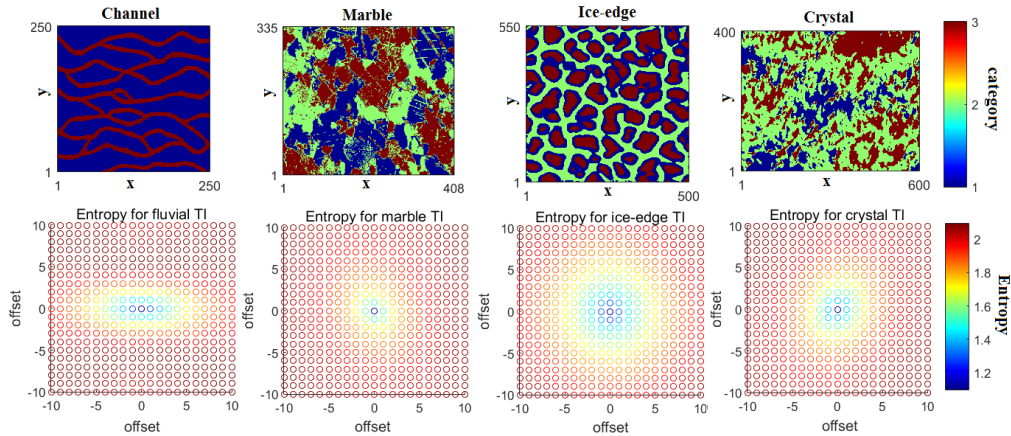


Figure 1.5: Four examples of entropy-based templates for TIs

1.6 MPS Assessment Approaches

1.6.1 Multiple Point Histogram (Clayton, 1992)

It is important to evaluate the realizations generated by MPS simulation. Multiple Point Histogram, abbreviated as MPHIST, is another way to quantify high order statistics. They count the frequency of patterns observed for an N-point configuration simultaneously. Figure 1.6 is an example 2×2 template situation computing the MPHIST. Consider a 4-point configuration where each location takes two possible categorical values, hence the total configurations are $2^4=16$, and the probabilities of finding them on a TI are given in Figure 1.6 (b). All of the configurations will be calculated on and the ordering of the configurations is arbitrary.

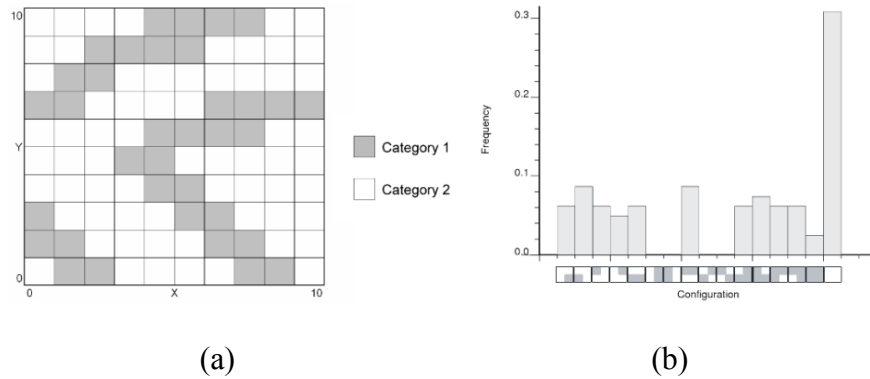


Figure 1.6: An example of a four-point configuration with 2 categories, generating 16 classes of combinations and is scanned over a TI (Boisvert et al., 2006).

The idea of using MPHIST to judge the realizations is based on computing the differences of MPHIST between the realizations to its TI, over non-repeated portions, as given in Equation 1.7. Where i is the bin number, m is the maximum number of bins, f_i^{Real} is the frequency corresponding to bin i for the realization, and f_i^{TI} is the frequency corresponding

to bin i for the TI. The larger the $diff$ is, the more differences between the realizations to the TI.

$$diff = \sum_{i=1}^m |f_i^{Real} - f_i^{TI}| \quad \text{Equation 1.11}$$

1.6.2 Distribution of Runs (Mood, 1940)

The distribution of runs accounts for the connectivity of adjacent points in a line or runs. It was used in the content of assessing MPS to select TIs by Boisvert et al., (2007). An example below shows how the distribution of runs is computed. Consider a following sequence between $[0, 1]$ that are coded for three thresholds of 0.25, 0.5, and 0.75:

0.15 0.21 0.24 0.55 0.38 0.71 0.66 0.45 0.58 0.47 0.13 0.36 0.91 0.82

$Z_1=0$ 0 0 1 1 1 1 1 1 1 0 1 1 1 1

$Z_2=0$ 0 0 1 0 1 1 0 1 0 0 1 1 1 0

$Z_3=0$ 0 0 1 0 0 0 0 0 0 0 0 1 1 0

Code the value above the threshold as 1, 0 as below the threshold. The definition for a run of length L above the threshold z_k is a sequence of $L+2$ adjacent nodes with the same indicator value except for the first and the last nodes. As in that case the sequence is coded as:

- A run above the threshold $Z_1=0.25$ is length of 7;
- A run above the threshold $Z_2=0.5$ is length of 3;
- A run above the threshold $Z_3=0.75$ is length of 2;

The same concept can be applied to below the threshold. Other than that, the runs can be cumulative with more than one type of length.

In 2D realization assessment, distributions of runs are calculated for both x-z and y-z direction. Once the cumulative distributions of runs for the selected realizations are obtained they are able to be compared with each other. The differences between distributions on each direction can be calculated as:

$$diff = \sum_{l=1}^n |f_l^1 - f_l^2| \quad \text{Equation 1.12}$$

Where *diff* is the difference between the distributions; *l* is the length of runs; *n* is the maximum length of runs; f_l^1 is the cumulative frequency of realization for runs length of *l*, and f_l^2 is the cumulative frequency of TI for runs length *l*. The smaller the difference is, the more similar two patterns are.

1.6.3 Multidimensional Scaling

Multidimensional scaling (MDS) is implemented in MPS as a technique to describe patterns along a set of dimensions as points in multidimensional space. The dissimilarity between patterns can be simply represented by distances of the corresponding points in the multidimensional space. Scheidt and Caers (2007) proposed the Distance Kernel Method (DKM) to identify several typical realizations and then cover the spread of uncertainty accurately by only performing a small number of simulations.

The dissimilarity matrix and dissimilarity distance function are explained as follow: Dissimilarity matrix is a matrix that measures the difference from one region of the image to another. The function to calculate the dissimilarity between patterns is called the dissimilarity distance function. The first content to link this concept to MPS information was presented by Arpat (2005), Suzuki and Caers (2006). The dissimilarity matrix is computed by a Euclidean distance due to its simplicity. Defining two patterns from the

image $patdb_T$ as pat_T^m , pat_T^n , and the Euclidean distance $d_E(x,y)$ between two patterns is shown in Equation 1.9:

$$d_E\{pat_T^m, pat_T^n\} = |pat_T^m - pat_T^n| \quad \text{Equation 1.13}$$

Euclidean distance is the summation of pixel-wise differences. In Chapter 2, the dissimilarity matrix is applied to assess stationarity.

1.7 Hierarchical Simulation

As the number of categories in the TI increases, the general MPS simulation procedure is confronted with an issue that fewer replicates are found in the TI. The hierarchical approach is used as a potential solution to solve the disadvantages of simulating too many categories all at once. The key idea of hierarchical simulation is to re-create the TI based on its geological or statistical ordering, and then simulate in a series of steps. Many previous works proved the advantages of hierarchical approach on models with large amount of categories. Strebelle (2000) introduced a hierarchical approach to simulate four fluvial categories including channels, levees, crevasse splays, and floodbasin. Maharaja (2004) explains the process of the hierarchical approach in detail, and then implemented the method to models with three and four categories respectively, based on their geologic rules of deposition. Lyster (2004) used the hierarchical method to simulate a rock model with five rock types and generated reasonable realizations. Chapter 5 focuses on the implementation of hierarchical simulation to a variety of TIs, summarizing practical rules for practitioners.

1.8 Thesis Outline

Chapter 2 will assess the stationarity scores of ten 2D TIs and six 3D TIs by the category distribution, the oriental estimation including “normality”, “uniformity”, and “repeatability”, as well as the Euclidean distance computing the distance between sub-regions from a TI. Chapter 3 and Chapter 4 will implement a large number of SNESIM simulations and summarize the optimal settings for generating well reproduced realizations. Chapter 4 will also apply and compare the influence of different data spacing on 3D model. Chapter 5 will discuss about another approach of MPS simulation, hierarchical simulation, and sum up for rules about how to perform the lumping and how to generate good realizations. The workflow of hierarchical simulation, the categorical relationship calculating related programs and updated hierarchical SNESIM program are presented in Appendix.

Chapter 2

Stationarity of Various TIs

2.1 Training Images

Pyrzcz, Boisvert and Deutsch (2008) published a TI library of fluvial and deepwater reservoirs. Another public TI library was presented by Mariethoz (2014), which includes TIs that vary from oceanic to basin reservoirs. 16 TIs of different types are introduced in this chapter, ranging from mining to hydrology, and are tested for stationarity. It is proposed that the stationarity of TIs affects the quality of simulation directly. Poorly stationary TI is difficult to generate reasonable realizations, because of many non-repetitive features that render too many patterns in that size of the TI. Ten 2D TIs are shown in Figure 2.1: (a) a channel TI (Strebelle, 2002), the dimension of which is 250×250 cells; (b) a simple TI with two categories from the TI library (Mariethoz & Caers, 2014), of simulation grid 100×100 cells; (c) is a scanned picture of rock surface (Deutsch), 300×200 cells; (d), (e), and (f) are 3-category TIs from the report (Meerschman, et al., 2013), specifically, where (d) is a microscopic view for a thin marble slice, of size 408×335 cells; (e) an image of ice-edge polygons with dimension of 500×550 grid cells; (f) an image of snow crystals in 600×400 cells; (g) is another TI with a dimension of 400×400 cells, collected from the Walker Lake (Mariethoz & Caers, 2014) exhaustive DEM dataset; (h) is a porphyry reservoir TI with four rock types in a dimension of 100×100 cells (Silva, 2014); (i) is a TI with 5 categories (Lyster, 2004) with five categories in 200×100 cells, and (j) is an 8-

category non-stationary TI from Straubhaar et al., (2013) with a dimension of 400×100 cells.

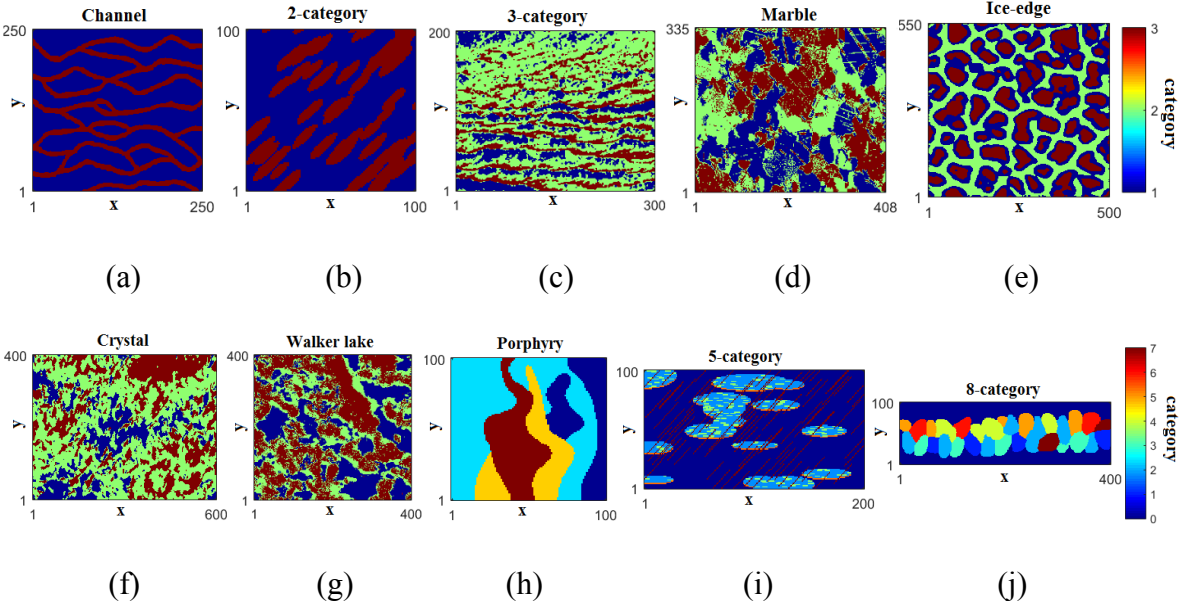


Figure 2.1: 2D TIs: (a) channel TI (Strebelle, 2002); (b) TI with two categories (Mariethoz & Caers, 2014); (c) scanned rock surface (Deutsch); (d) marble TI (Meerschman, et al., 2013); (e) ice-edge TI (Meerschman, et al., 2013); (f) crystal TI (Meerschman, et al., 2013); (g) Walker Lake (Mariethoz & Caers, 2014); (h) porphyry TI (Silva, 2014); (i) 5-category (Lyster, 2004); (j) 8- category TI (Straubhaar et al., 2013)

Two-dimensional TIs are easy to obtain through digitized photographs of geological outcrops or even a sketch drawn by a geologist. One issue in the application of MPS is the lack of appropriate 3D TIs. One method suggested by Strebelle (2012) to obtain 3D TIs is to generate unconditional realizations using the plan view and cross-section view offered by users. Comunian et al., (2011) implemented 2D TIs that perform 3D simulations. Through personal communication with Renard and Strebelle, six 3D reservoir TIs are collected. Figure 2.2 presents six categorical 3D TIs: (a) is a deepwater turbidite reservoir, mimicking

a West African modeling project with a dimension of $119 \times 69 \times 14$ grid cells; (b) is a tidal-dominated reservoir with five categories, with a dimension of $149 \times 119 \times 15$ cells; (c) is a carbonate reservoir, with cell grids of $90 \times 99 \times 22$; (d) is a fluvial-deltaic reservoir also from the West African modeling project with a dimension of 70 by 183 by 20 simulation grids; (e) and (f) are object-based models from the west coast of Africa from the TI library (Mariethoz and Caers, 2014). West coast data I (e) and II (f) both have dimensions of $78 \times 59 \times 118$ cells.

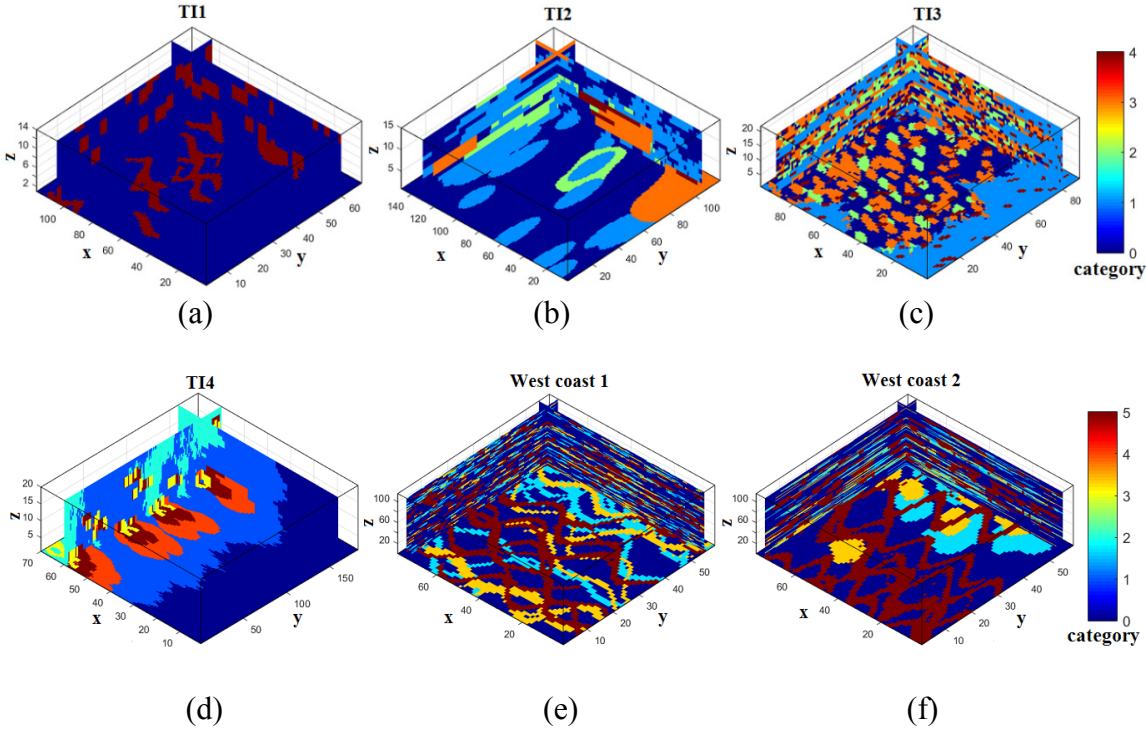


Figure 2.2: 3D TIs: (a) turbidite reservoir (Strebelle, 2005); (b) tidal-dominated reservoir (Strebelle, 2005); (c) carbonate reservoir (Strebelle, 2005); (d) fluvial-deltaic reservoir (Strebelle, 2005); (e), (f) west coast of Africa (Mariethoz and Caers, 2014)

2.2 Stationarity Tests

Stationarity defined here is not the conventional concept of stationarity of a random function; stationarity in this work considers the repetition of patterns in a TI, representing the quality of the TI. One detailed and clear guide about assessing the stationarity of TIs was presented by Mirowski, et al., (2009). Three methods of measuring scale property field of TIs, the category distribution, orientation property field were introduced for evaluating TIs. The scale method is an image-processing technique, based on extracting a reference pattern (a small sample of the image) from each of nine sub-regions of the image. The reference pattern is successively stretched or compressed along two main axes, and then be compared to other samples of the image.

The second stationarity test is to quantify the orientation of local shapes, which is defined as the preferential direction of the local features in a TI. The similarity of the circular statistical distribution is measured as stationarity scores between pairs of sub-regions to obtain an overall estimate of variation of orientation over the TI. In conclusion, TIs that yield high stationarity scores show more constant properties spatially, and those with low scores tend to be less stationary. The category distribution and orientation assessment are discussed in this chapter.

2.3 Methods for Assessing Stationarity

Four approaches are implemented to test for the stationarity of the TIs: the three types of stationarity scores introduced above; and MPHIST, an extension of the univariate histogram, presented for counting frequency of all possible configurations that simultaneously appear in an image. The main purpose is to check for repeatability and similarity through every subset of the TI. In this thesis, the 2D TIs are divided into 9

overlapping zones as $\{Z_i, i=1, \dots, 9\}$ (Figure 2.3). Each zone takes up a quarter of the TI, representing the “top,” “left,” “right,” “bottom,” “center,” and four corners of the TI. All sub-regions are compared pairwise summing for the overall difference, which accounts for the TI’s stationarity level. The statistical results are sorted in a descending order given in Table 2.1.

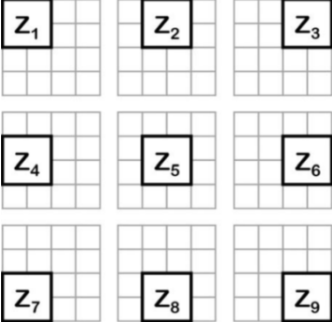


Figure 2.3: An example of decomposing a 2D TI into 9 sub-regions (Mirowski, et al., 2009).

2.3.1 Category Distribution

All of the TIs used are categorical; therefore, the first statistic tested for stationarity is the proportions, which quantifies how the proportions of categories vary from one region of the TI to another. The less the distribution changes, the higher the stability and stationarity of the image is. As the subsection example given in Figure 2.3.1, 9 sub-zones yield 36 couples of zones to be compared. More specifically, the first step is to transform the TI into binary images if the number of categories is greater than two (Figure 2.4).

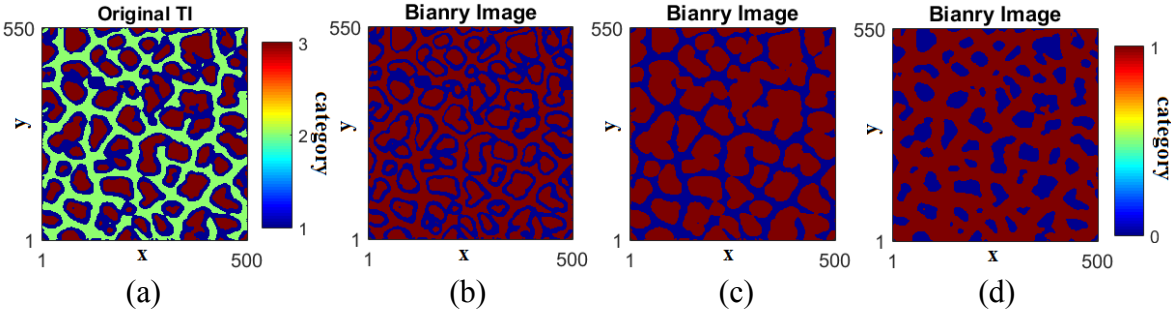


Figure 2.4: An example of merging categories: (a) TI with three categories; (b), (c) and (d) are transformed binary TIs presenting the categories individually.

The normalized histograms for each category within each zone \mathbf{i} and \mathbf{j} , H_i and H_j are then computed. The similarity for two categories of their histograms is measured using the Euclidean distance between vectors H_i and H_j (Equation 2.1). The number of 2D combinations is $C_9^2 = 36$, and for 3D is $C_{27}^2 = 351$.

$$D(\mathbf{i}, \mathbf{j}) = \sqrt{[H_i(k) - H_j(k)]^2} \quad \text{Equation 2.1}$$

Where $\sum_{k=1}^K H_i(k) = 1$, $\sum_{k=1}^K H_j(k) = 1$, K is the number of categories, and k is the current category. Finally, the category distribution stationarity score for is defined by summarizing the category distribution from all of the zones:

$$\text{category_score} = 1 - (1, \min(\text{sum}\{D(\mathbf{i}, \mathbf{j})\})) \quad \text{Equation 2.2}$$

Figure 2.5 is an example of categorical histograms of three rock types distributed within each zone. The TI is divided into 9 zones, and bars around represent the distribution of categories within that zone. Table 2.1 at the end of this chapter compares the category distribution testing results for eight 2D TIs in descending order. However, the exact cut-offs to assess stationarity are uncertain only by calculating the statistics. The unconditional simulation realizations of TIs are compared in the next chapter in order to determine appropriate cut-offs. The original work of the category distribution refers to the content of Mirowski et al., (2009).

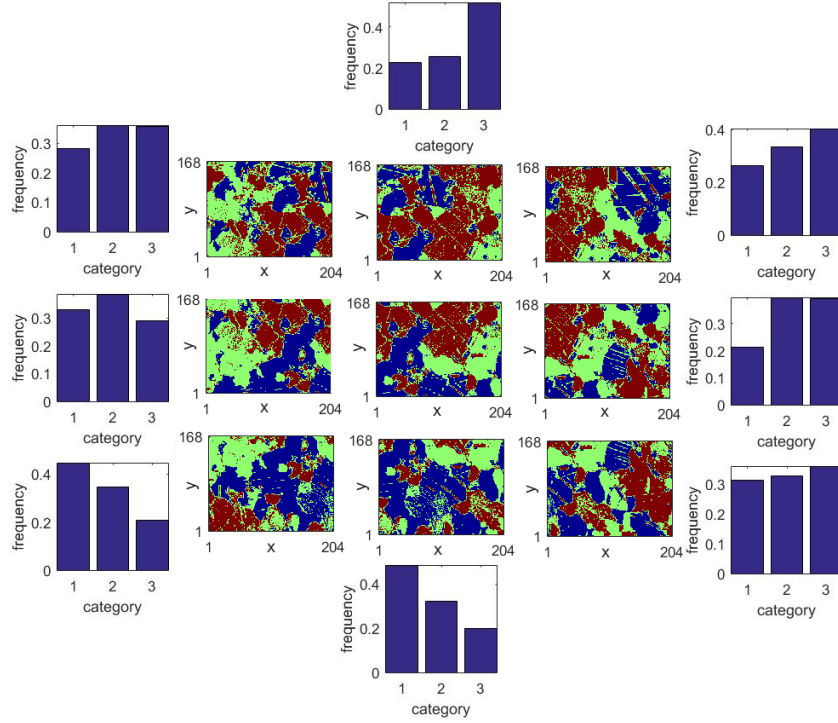


Figure 2.5: An example of category histograms for subsections of TI with 3 rock types.

2.3.2 Orientation Stationarity

This method is referred to in Mirowski et al., (2009). Orientation stationarity aims to quantify the consistency of the orientation of features in the TI. This is estimated through three auxiliary scores: normality, which quantifies whether the distribution of orientation is approximately a von Mises distribution, which can be considered as the Normal distribution of circular data; non-uniformity, which verifies whether the circular distribution of angles is uniform under the von Mises assumption; and repeatability, which accounts for the difference between two circular distributions. Three auxiliary scores all relies on the assumption of von Mises distribution, therefore they are employed together as a measure to judge the shape or local preferential orientations of the circular distribution. The probability density function of the von Mises distribution is given in Equation 2.3:

$$f(a; \theta, \kappa) = \frac{1}{2\pi I_0(\kappa)} \exp[\kappa \cos(a - \theta)] \quad \text{Equation 2.3}$$

Where θ is the mean direction of the distribution in the range $[0, 2\pi]$, and κ is the concentration parameter. As shown in Figure 2.6, when κ is zero, the von Mises distribution reduces to the uniform distribution. When κ increases, the von Mises distribution approaches the normal distribution.

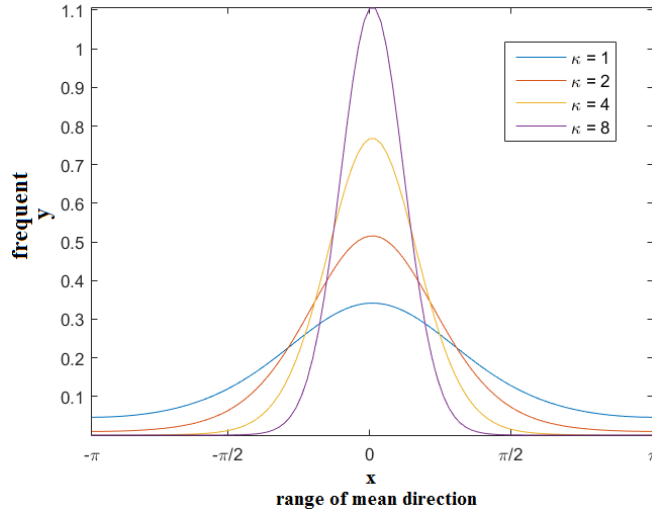


Figure 2.6: PDF of von Mises distribution

The first be tested is normality. Normality is based on a goodness-of-fit Chi-Square test verifying the assumption of the axial von Mises circular distribution of angles. The normality is defined as:

$$\text{normality}_{2D} = \frac{\alpha_{ii}^1 + \sum_{k=1}^9 \alpha_{z_k}^1}{10} \quad \text{Equation 2.4}$$

Experience suggests that when κ value is larger than 20, $\alpha=100\%$ confidence level is automatically achieved (Mirowski et al., 2009).

The second test is non-uniformity (Mirowski et al., 2009). Uniformity occurs when all values around the unit circle are equally alike. The Rayleigh test, relying on the assumption

of von Mises distribution, is used to complete the test. If the result shows a small p-value, which indicates a significant departure from the uniformity, the null hypothesis is rejected.

Non-uniformity is defined in Equation 2.5:

$$\text{nonuniformity}_{2D} = \frac{(1 - \alpha_{ii}^2) + \sum_{k=1}^9 (1 - \alpha_{z_k}^2)}{10} \quad \text{Equation 2.5}$$

The third test is repeatability, which quantifies the similarity between a pair of circular distributions of two sub-regions from the image (Mirowski et al., 2009). This score relies on the similarity test for all possible pairs of distributions and is defined as:

$$\text{repeatability} = \frac{\sum\{u \in [1,9]\} \sum\{v \in [1,9]\} \delta_{uv}}{C_9^2} \quad \text{Equation 2.6}$$

$$\delta_{uv} = \begin{cases} 1 & \text{if } \alpha_{z_u, z_v} > 0.05; \\ 0 & \text{otherwise} \end{cases}$$

Where α_{z_u, z_v} is drawn from the nonparametric Watson two-sample U^2 test (Mardia, 1972, pp. 201-203), and if it is larger than 0.05, the δ_{uv} will be 1, which renders the repeatability between two zones u and v is 1, otherwise it is 0. The experienced final orientation stationarity score can be computed by partially adding up the three auxiliary statistics scores after all they are known as given (Equation 2.7):

$$\text{orientation_stationarity} = \frac{1}{4} \text{normality} + \frac{1}{4} \text{nonuniformity} + \frac{1}{2} \text{repeatability} \quad \text{Equation 2.7}$$

All of the related calculations are done using a MATLAB toolbox for circular statistics (Berens, 2009). Results of all scores for the selected TIs are collected in Table 2.1.

2.3.3 MPHIST

As discussed in Chapter 1, the MPHIST is a commonly used high-order statistics distribution. In this chapter, Δ MPHIST between each pair of subsections are computed and

summed to assess pattern stationarity. The same template is kept for consistency. The smaller overall difference, the more stationary the TI is. All of the results for each TI are presented in Table 2.1.

2.3.4 Distance Matrix

The Euclidean distance, presented in Chapter 1, is employed to assess the similarities over subsections of a TI. Distances are presented in dissimilarity matrix, which is summarized to quantify the stationarity. The larger this summation is, the less stationary of the TI. Stationarity calculation consequences are shown in Table 2.1.

2.3.5 Final Results

The final results of all four methods are presented in Table 2.1. Green values indicate better stationary scores, red represents for poor stationarity. Considering the highest value as a standard within each row, results falls into three intervals that are either higher than the 2/3 of the highest value, or lower than 1/3 of the highest value. MPHIST results of porphyry data is an exception, because this TI is highly non-stationary for the method, hence it is not used as a standard.

The channel TI and the 2-category TI are highly stationary, since they both have high scores. Rock surface and 5-category TI are determined to be in the middle because they both have some good or poor results and usually medium values. The statistics of the 8-category TI indicate its poor stationarity, since the features are complex and various. The stationarity for rest of the TIs are considered to be uncertain, since they all have good and poor results, which cause difficulties in judging their stationarity. It can be seen from the table that distance matrix is not a very good method, because the results are different than other methods. The final stationarity levels and exact cuts-off between stationary and non-

stationary TIs is the focus of Chapter 3 when realizations are created to assess how well each TI performs in simulation.

Table 2.1 (a): Stationarity calculation results for four methods

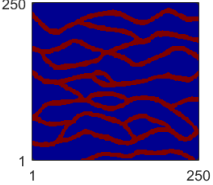
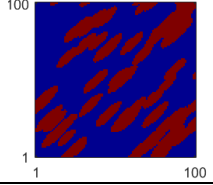
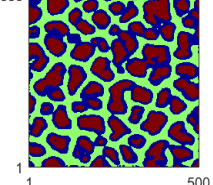
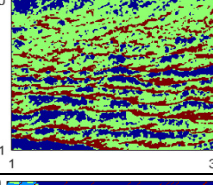
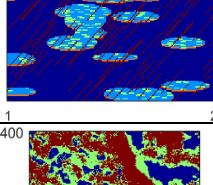
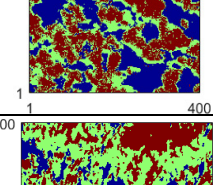
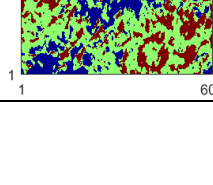
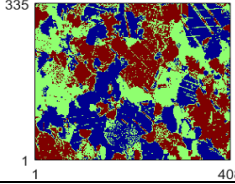
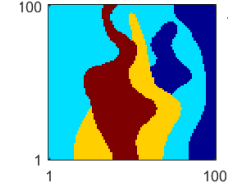

TI	Category distribution	Orientation	MPHIST	Distance	Stationarity level
	0.89	47.3	0.22	2875.90	Good
	0.77	38.9	0.28	1221.40	Good
	0.87	54.4	0.28	10924.11	Uncertain
	0.77	28.8	0.19	4141.59	Medium
	0.59	39.7	0.13	4495.12	Medium
	0.69	28.6	0.11	8333.03	Uncertain
	0.64	29.8	0.16	8676.41	Uncertain

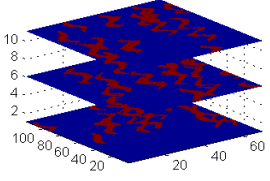
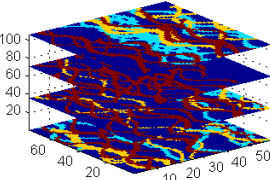
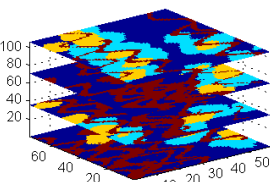
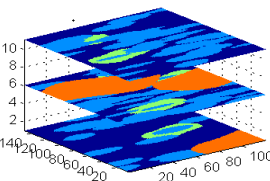
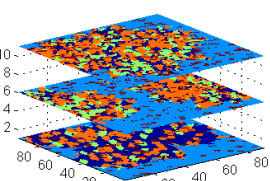
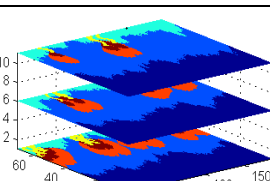
Table 2.1 (b): Stationarity calculation results for four methods

TI	Category distribution	Orientation	MPHIST	Distance	Stationarity level
	0.59	32.3	0.19	7795.64	Uncertain
	0.15	29.8	2.23	2718.32	Uncertain
	0.31	27.5	0.56	11465.56	Poor

2.4 3D TIs Stationarity Tests

Assessing the 3D TI stationarity follows the same procedure as introduced before, but the TI is divided into three layers along the vertical direction, hence the number of pairwise combinations is 351. The results of the category distribution, MPHIST and distance matrix are presented in Table 2.2. The channel TI is highly stationary, for all of the evaluation scores are showing high values. West coast TIs are both uncertain since they both have poor and good results. The stationarity of the TI4 is poor because it has a strong trend. The category distribution and MPHIST results are quite poor expected with such a trend. The other two models are uncertain due to their average scores. The third column, Euclidean distance still shows different results than other methods, the stability of this method will not be discussed in this thesis again.

Table 2.2: Stationarity test results for 3D TIs

TI	Category distribution	MPHIST	Distance	Stationarity level
	0.77	0.08	25277.59	Good
	0.77	0.03	170848.07	Uncertain
	0.5	0.08	169995.94	Uncertain
	0.55	0.57	109709.74	Medium
	0.46	0.1	99830.89	Medium
	0.1	16.3	93047.73	Poor

2.5 Discussion

Four methods, including category distribution, orientation stationarity, MPHIST, and distance matrix to test for the stationarity of TIs, are discussed. The category distribution quantifies how categories vary from one region of the TI to another. The orientation stationarity estimates consistency of the orientation shapes in the TI, which is measured by normality, uniformity of circular distribution and repeatability of features. Differences in MPHIST use a small template to scan different zones and capture their frequencies. Finally, the Euclidean distance is calculated to quantify the dissimilarity between sub-regions. Within each method, the highest value is considered as a standard to measure stationarity level.

Four assessment results are compared with each other. Category distribution, orientation, and MPHIST show similar results, but the distance matrix is not convincing enough since it relies on the proportions of categories in TIs and the translation of features, and will not be used to assess stationarity in following content. If the testing results are consistent, stationarity of the TI can be assessed. However, some TIs are uncertain due to different calculation results, which require further study in following chapters. Therefore, in addition to statistics, the performances of unconditional simulation in Chapter3 and Chapter 4 will further assess TI quality, as well as the exact cut-off to define the stationarity level of 2D and 3D TIs for each matrix.

Chapter 3

Optimization of MPS Simulation Parameters

3.1 SNESIM Simulation

SNESIM is introduced in Chapter 1, which is a popular approach used in MPS modeling. SNESIM approach is used to generate MPS realizations throughout this thesis. To determine the optimal settings of MPS simulation, and to acquire the better reproduction from TIs, sensitivity tests are conducted on the following parameters: the number of points in a template; the type of template; the number of multiple-grids; the number of search trees, and; the amount of conditioning data. Realizations are evaluated both visually and statistically. The ten 2D TIs introduced in Chapter 2 are tested with the SNESIM algorithm. Realizations are compared to identify the common SNESIM parameters that result in good TI feature reproductions. The stationarity of the TI is assessed again considering the quality of the realizations, and the cut offs for determining the quality of the TI is provided at the end.

3.2 Template

The template is a major influence on SNESIM simulations. Two types of template are compared. The entropy-based template generation theory was introduced in Chapter 1. The first type of template that will be applied is the entropy-based template (Lyster, 2009). Figure 3.1 presents examples of the entropy-based templates generated from eight TIs. The blue points in the middle the lowest entropy locations that indicate few randomness, and the yellow points around increase to higher entropy. A template that consists of points with more information can better capture the features of a TI. Distribution of entropy values

corresponds mostly to the orientation of major objects. For example, the distribution of entropy values for the porphyry TI is an ellipse along the N-S direction, which is close to the shape of the major categories.

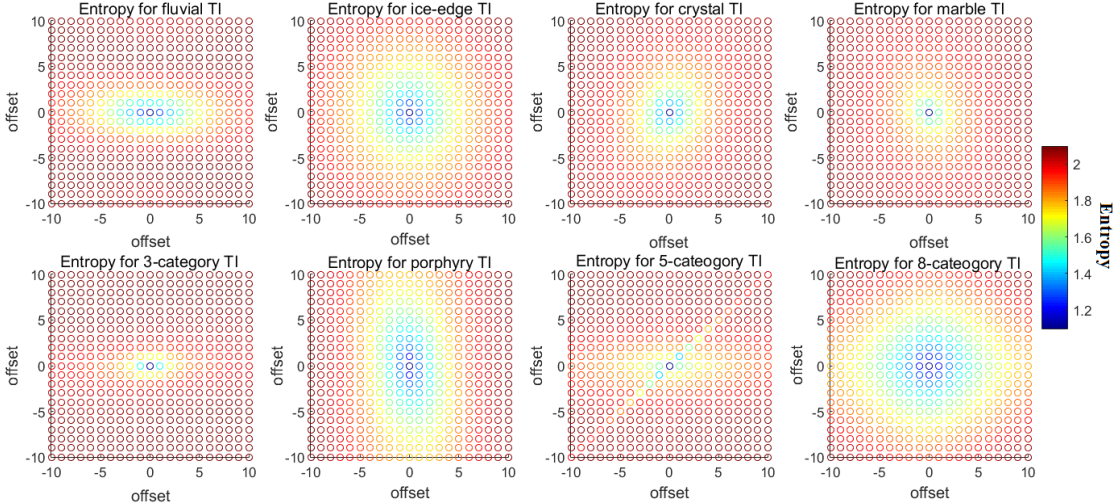


Figure 3.1: Eight examples of entropy-based templates

Template sizes vary from 10 to 100 points, and they are selected from the central location of the highest entropy of the corresponding TI. At the same time, the number of multiple-grids changes from one (finest) to five successively. The differences in MPHIST between realizations and TI are computed and presented in Figure 3.2. Figure 3.2 shows the results of simulating 12 TIs in different situations. The first observation is that when the number of multi-grids increases from one to three, Δ MPHIST decreases rapidly for all TIs (Figure 3.4). Meanwhile, most of the Δ MPHIST results are reduced quickly when the number of points increases from 10 to 60, and eventually, there is little gain in realization quality for many points.

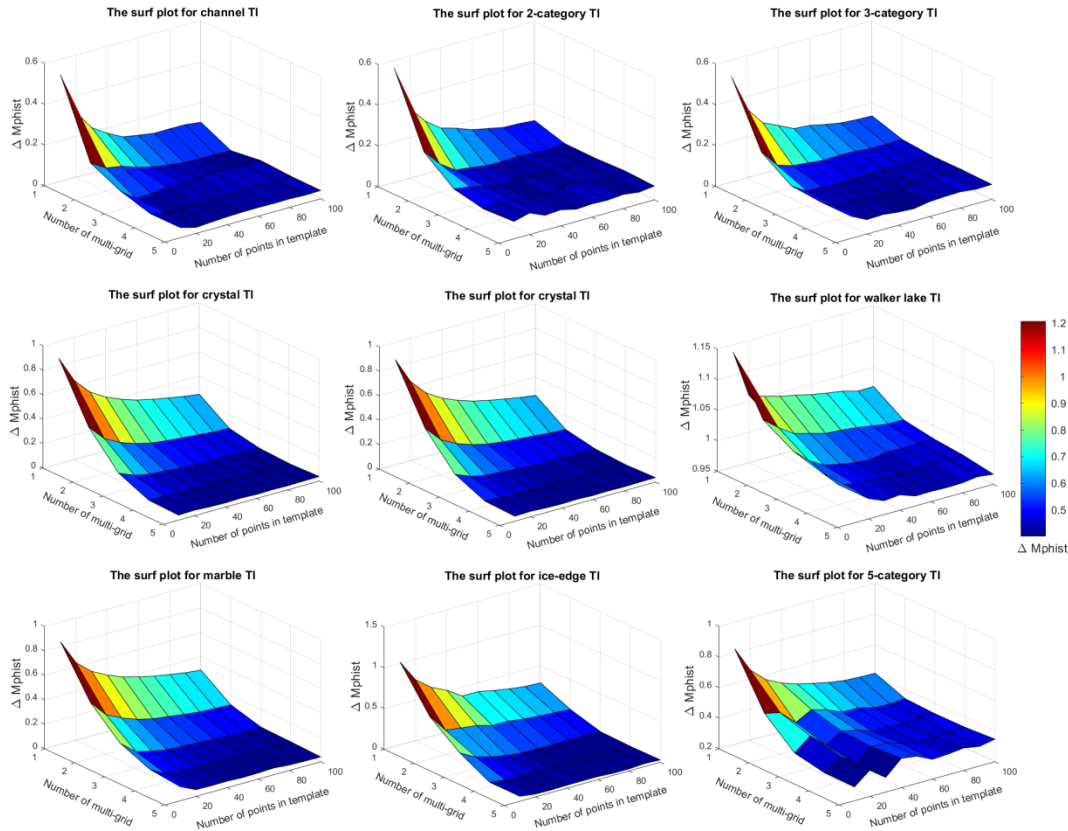


Figure 3.2: 3D surface plot of the size of the template, the number multi-grids, and Δ MPHIST

Figure 3.3 compares the Δ MPHIST values when using 10 different template sizes with four and five multi-grids. Six TIs that are more stationary have a lower Δ MPHIST than the four other less stationary TIs; therefore they are plotted separately. The lowest Δ MPHIST for most TIs appear between 40 to 70 template points. One fact to notice is that after a large size of template, the descending trend turns flat. The reason is that the farthest datum can be dropped during simulation when not enough replicates are found, then the size of template actually used is smaller than the input template. The three lowest Δ MPHIST are the channel TI, the 3-category TI and ice-edge TI. The template size does not significantly influence the simulation for Walker Lake data, porphyry, 5-category and crystal TI. The reason that small

template works better is that the TIs (5-category and 8-category TI) are made up of many tiny objects. It is difficult to replicate very small-scale features from a TI when using large templates and relatively small TIs.

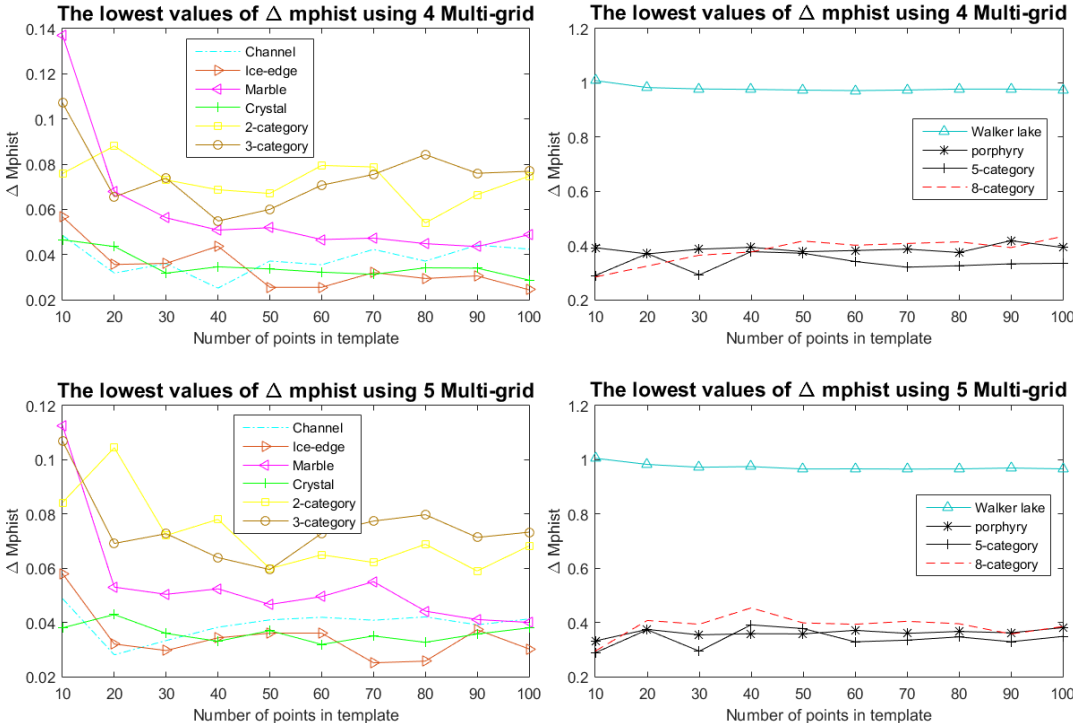


Figure 3.3: Δ MPHIST results for 10 templates with 4 and 5 multi-grids

Figure 3.4 shows the powerful influences of multi-grids on simulation. Realizations in Figure 3.4 are disordered when only one or two multi-grids are used, because the program simulates directly on the finest grid instead of simulating only progressively to the finest grid. Therefore, the large-structure features cannot be captured. Consequently, the best application is to set up a large number of multi-grids with a minimum number of 4.

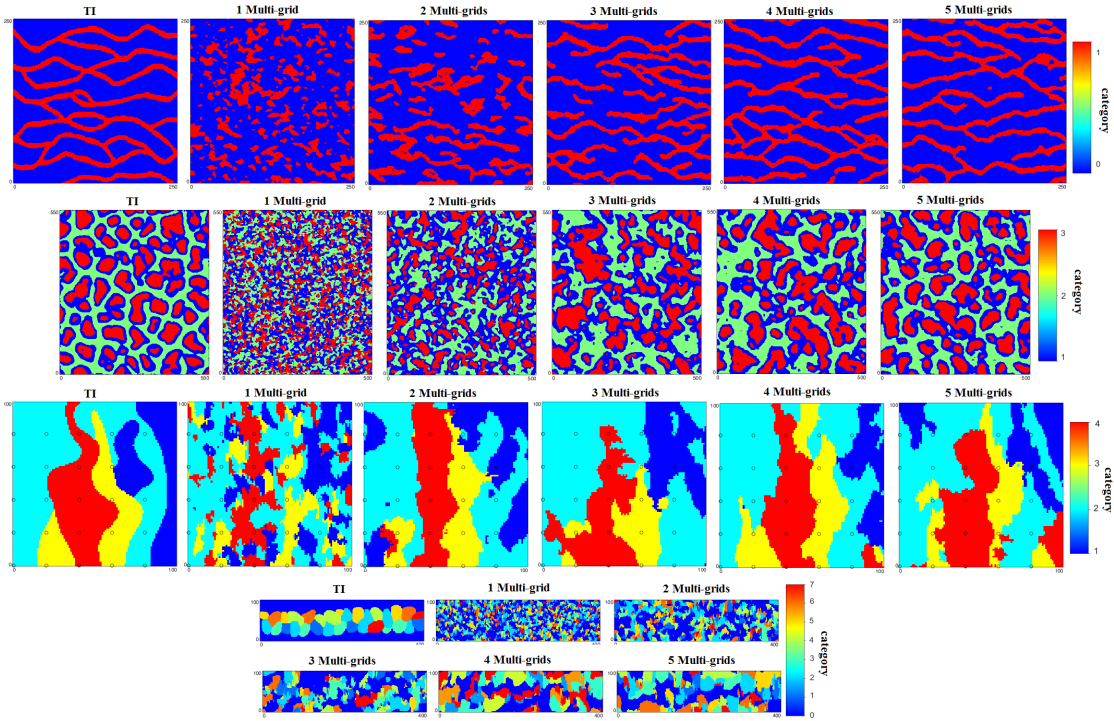


Figure 3.4: Realizations using different numbers of multi-grids.

Another aspect of the template that influences simulation is its shape. The regular-shaped templates are compared with the entropy-based templates. Figure 3.5 shows eight regular-shaped templates that will be used for all of the TIs. They are comprised of 20, 21, 24, 25, 44, 48, and 80 points respectively. The same sizes of entropy-based templates are compared to these templates, in order to determine the influence of template shape.

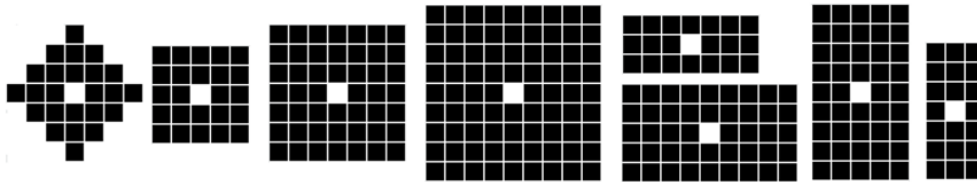


Figure 3.5: Eight examples of square- and rectangular-shaped templates

Figure 3.6 (a) compares the results of using regular-shaped templates. As the number of categories in the TI increases, there is a greater chance that the realizations results in a

higher value of ΔMPHIST , because there are more potential patterns in the MPHIST. Figure 3.6 (b) shows the result of using the entropy-based template, which is more stable without fluctuations compared to Figure 3.6 (a), because the templates are consistent. 8-category TI prefers a 7×7 square template than an entropy-based template, and the result is the same for the 3-category TI. The two figures suggest that good results do not always occur when applying an entropy-based template, and whether regular or entropy-based templates actually render similar results on ΔMPHIST . The 3-category and channel TI do not change much through all the templates. In general, the template shape does not have a large effect on feature reproduction.

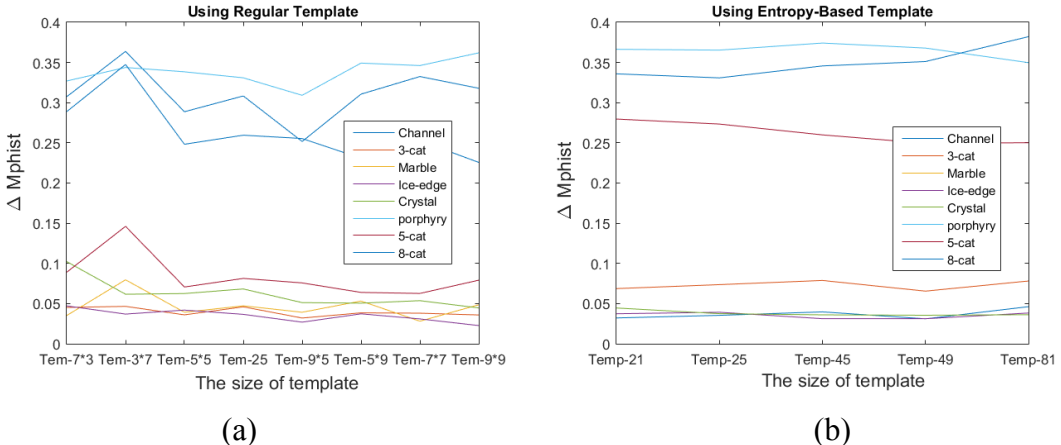


Figure 3.6: ΔMPHIST of two types of templates (a) ΔMPHIST of realizations of using templates with regular shape ; (b) Entropy-based template using between 21 and 81 points.

Some recommendations can be drawn from this sensitivity analysis:

1. Four or five multi-grids are recommended for all TIs.
2. An entropy template within a size of 40-70 can be applied to most 2D TIs with large templates, but in general the template shape does not have a large effect on feature reproduction. Because the farthest datum can be dropped if not enough replications

are found, the size of template used in actual simulation can be smaller than input template. TIs (5-category and 8-category) with tiny objects, a small template works better.

3. As expected, TIs with a number of categories ≥ 4 results in worse feature reproduction as the TIs were all approximately the same size and there are more patterns in a TI with more categories.
4. Square-shaped templates are usually preferred over rectangular ones. A template size 9×9 works well for most 2D TIs.

3.3 Assessment of Geostatistical Realizations

Multiple realizations are always generated during MPS simulations. Because the quality of the realizations represents the quality of parameter settings, it is important to determine an appropriate approach to analyze the realizations. It is not proper to use the conventional first and second order statistical approaches, including variograms, to assess MPS realizations, because the variogram is not the concern of MPS. MPHIST is chosen for the MPS assessment because it considers multiple point information. The application of MPHIST to rank realizations was proposed by Boisvert et al., (2006) in the content of comparing TIs and the realizations. As recalled in Chapter 1, while applying this technique in realization assessing, the same combination of templates are scanned over the TI. The lower the Δ MPHIST, the more similar the realization is to the TI and the better the reproduction of geological features. The following sections compare the distribution of runs, multidimensional scaling to Δ MPHIST results, in order to assess realizations using different metrics and to determine a better assessing approach.

3.3.1 The Distribution of Runs

The theory of distribution of runs is explained in Chapter 1. In a 2D realization assessment, distributions of runs are calculated in both x-z and y-z directions. Once the cumulative distribution of runs for the selected realizations is obtained, the realizations can be compared with each other. Figure 3.7 compares the distributions of along two directions of the realizations. When only looks at the statistics, porphyry and 8-category TI are much higher than others, which inform the weak stationarity, and the statistics of them are large in $\Delta MPHIST$ test in next section. Most of the TIs show a peak at the smallest rectangular template (3×7) along the y direction, which equals the results that are collected from the template test in Chapter 2. Differences in run distributions along the y-z direction that are higher than those along the x-z direction indicate that features along the north-south direction are not reproduced as well as those along the east-west direction. In comparison to $\Delta MPHIST$, the distributions of runs are found to be inferior, because they assess a string of values along one direction not a configuration with more diversity.

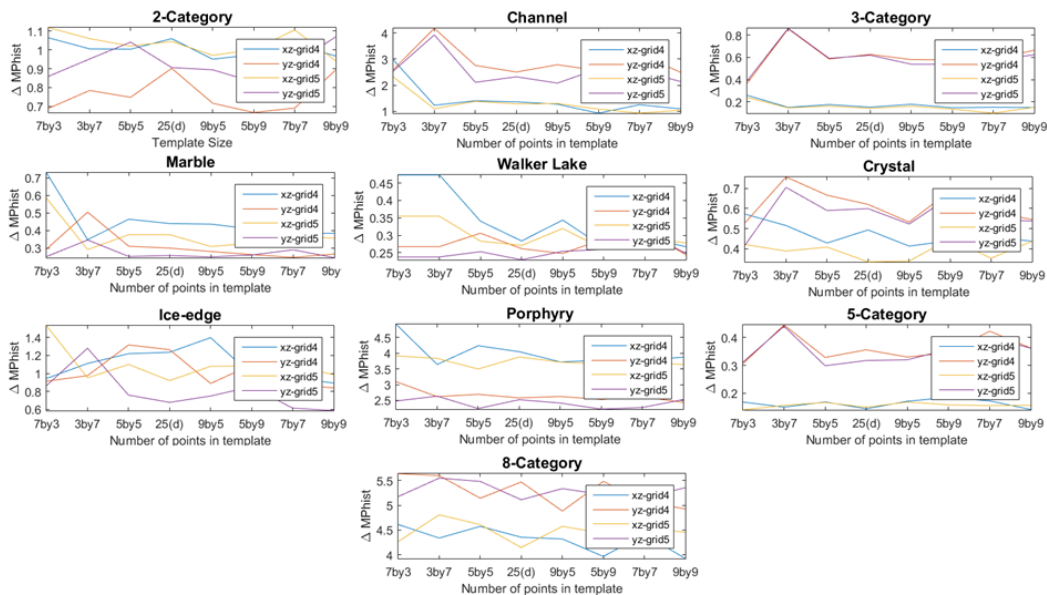


Figure 3.7: Results of the distribution of runs for 10 TIs using different templates.

3.3.2 Assessing Realizations using MDS

The introduction of implementing the MDS in the realizations assessment is discussed in Chapter 1. Here, MDS is assessed together with Δ MPHIST results together, to judge the quality of the realizations. The purpose is to find if the shortest distance between the realizations to the TI would match with the lowest value of the Δ MPHIST. If so, the scatters will be arranged along diagonal line. Every realization is calculated with MDS and Δ MPHIST. Multiple realizations are transferred to scatters in one multidimensional space. The value of Δ MPHIST is sorted with its corresponding classical MDS results in ascending order, in order to keep consistency with MDS results.

Table 3.1: Δ MPHIST in multidimensional space scatter plots and realizations comparison

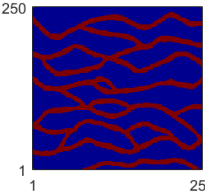
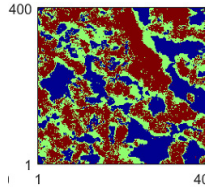
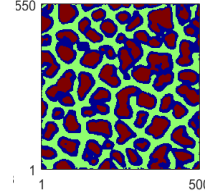
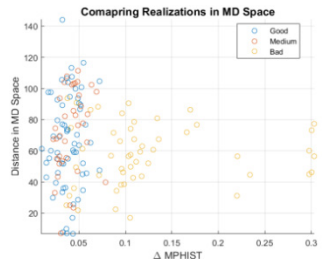
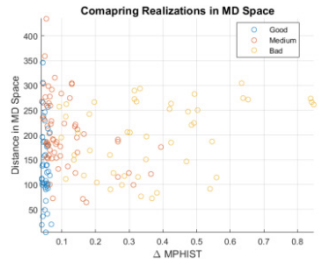
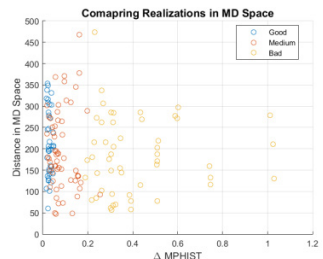
TI			
MDS vs MPHIST			

Table 3.1 illustrates three examples of comparing MDS results to Δ MPHIST. Each scatter in a scatter plot represents a location of a realization, and its value of Δ MPHIST and MDS. TI is the origin, while the realizations are blue, red and yellow scatters around. Blue points are “good-looking” realizations; Yellow points are poor realizations, and the red points are medium realizations. It can be found in Table 3.1 that scatters are not always follow the diagonal line, as well as others which are shown in this table. In addition, the value of MDS

is not necessarily low when the realization reproduces more features, or low when the realization has poor quality. Therefore, MDS is considered to be a not very convincing metric for assessing the realizations, and will not be implemented in the following content.

3.4 Assessing Stationarity

Table 3.2 assesses the quality of the stationarity of TIs. Unconditional realizations are generated from all TIs by applying the optimal parameters in SNESIM, including using 5 multi-grids, 50-point size of template, and search ellipses similar to the dimensional of the TIs, to calculate how well TIs perform. A visual comparison of the realization, group the realizations into three groups, good, medium, and poor. It can be seen from the table that TIs with good stationarity have well reproduced realizations, for example, the channel TI are well replicated; they are considered to have strong stationarity. 8-category and porphyry TI are poorly replicated; they are considered to have poor stationarity. The rest of the TIs are medium, because of the statistics calculated in Chapter 2 and the quality of the realizations are showing.

Table 3.2 (a): An assessment of TI stationarity

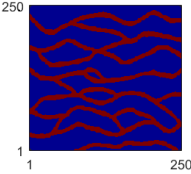
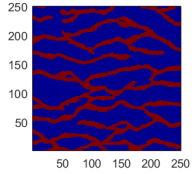
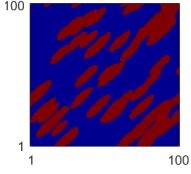
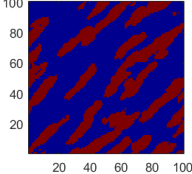
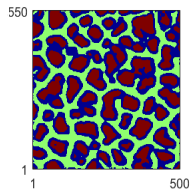
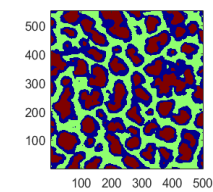
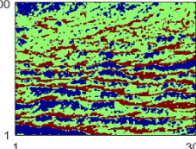
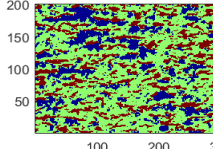
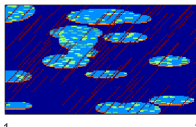
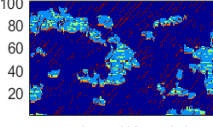
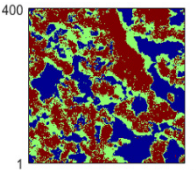
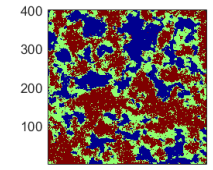
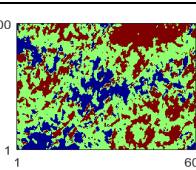
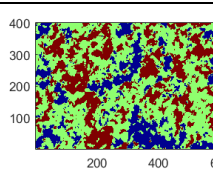
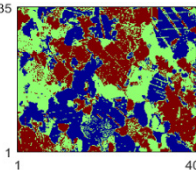
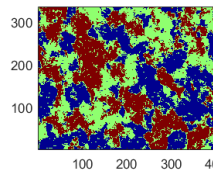
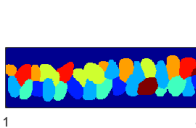
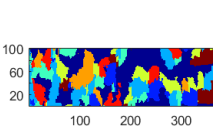
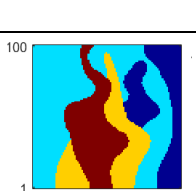
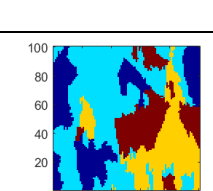
TI	Unconditional realization	Category distribution	Orientation	MPHIST	Stationarity level
		0.89	47.3	0.22	Good
		0.77	38.9	0.28	Good

Table 3.2 (b): An assessment of TI stationarity

TI	Unconditional realization	Category distribution	Orientation	MPHIS T	Stationarity level
		0.87	54.4	0.28	Good
		0.77	28.8	0.19	Medium
		0.59	39.7	0.13	Medium
		0.69	28.6	0.11	Medium
		0.64	29.8	0.16	Medium
		0.59	32.3	0.19	Medium
		0.31	27.5	0.56	Poor
		0.15	29.8	2.23	Poor

Cut-offs to determine the stationarity level using four methods are given in Table 3.3. The boundary value depends on the lowest (highest) value of the TI belongs to that group. For example, the lowest category distribution value of a TI in group “good” is 0.77, then the boundary to define “good” is 0.77. The highest category distribution of a TI in group “poor” is 0.31, then 0.31 is the boundary to define “poor”. The value in the middle defines the stationarity of “medium”. Statistical results, expect the “distance” results, are copied from Chapter 2.

Table 3.3: Cut-offs for stationarity level

Methods	Category distribution	Orientation	MPHIST
Good	> 0.77	> 38.9	< 0.28
Medium	0.31-0.77	29.8-38.9	0.28-0.56
Poor	< 0.31	< 29.8	> 0.56

3.5 Discussions

When implementing the SNESIM simulation, the template size for 2D TI should be over 40 points to get decent realizations; four or five multi-grids are highly recommended for accurate feature reproduction. TIs with strong stationarity can be well replicated through simulation. The differences in distribution of runs and the Δ MPHIST between realizations and TI are computed and compared to each other, as well as to the realizations themselves. The distribution of runs is found to be limited for only accounting for a string of dataset. MDS is compared to Δ MPHIST as well, trying to find if consistent with Δ MPHIST, but was failed at distinguishing quality of the realizations. Δ MPHIST is found to be a persuasive way to evaluate realizations, because of the quality of the realizations show matches the Δ MPHIST results. In addition, the quality of realizations also lies on the stationarity of the TI. Stationary TIs generate realizations that better reproduce the features

present in the TIs. A stationarity level of “good” refers to TIs with high statistical testing results that are within the defined cut-offs, and a high quality of the unconditional realizations; “poor” refers to non-repetitive structures shown in the TI, poor statistical results, and few feature reproductions in unconditional realizations; “medium” indicates that the TI is within medium stationarity level cut-offs, and the realizations have moderate feature reproductions of the TI. 3D TIs are discussed in the next chapter.

Chapter 4

Case Study of Assessing 3D TIs

4.1 Simulation of 3D TIs

4.1.1 SNESIM Simulation

The optimal selections of SNESIM parameters for 2D TIs were discussed in Chapter 3. The number of multi-grids has shown tremendous influences on qualities of the realizations. In this chapter, six 3D TIs (Figure 4.1), which have been introduced in Chapter 2, are implemented with 10 different sizes of templates, in order to analyze the influence of template and to determine an optimal size of the template for 3D TIs.

In addition, conditioning data play an important role in improving TI features reproduction, if the data conform to the TI features. Data spacing influences the behavior of simulations as well. The influences of the number of conditioning data on simulation are discussed in this chapter, by employing three types of drillings with data spacing of 10×10 , 20×20 , and 30×30 simulating cells between a pair of wells. Theoretically, the denser wells is, the better feature reproduced realizations are generated. Unconditional realizations are compared to conditional results in order to assess the importance of conditioning data, and the stationarity of TIs themselves. The realizations are compared visually and by Δ MPHIST.

The last section in this chapter is MPS simulation implementation on a large copper porphyry data, which is provided and introduced by Verly et al., (2009). The case study is testing the optimal settings summarized from the results of six 3D TIs simulation, and to look for a possibility for performing MPS simulation on a complex TI like the copper data.

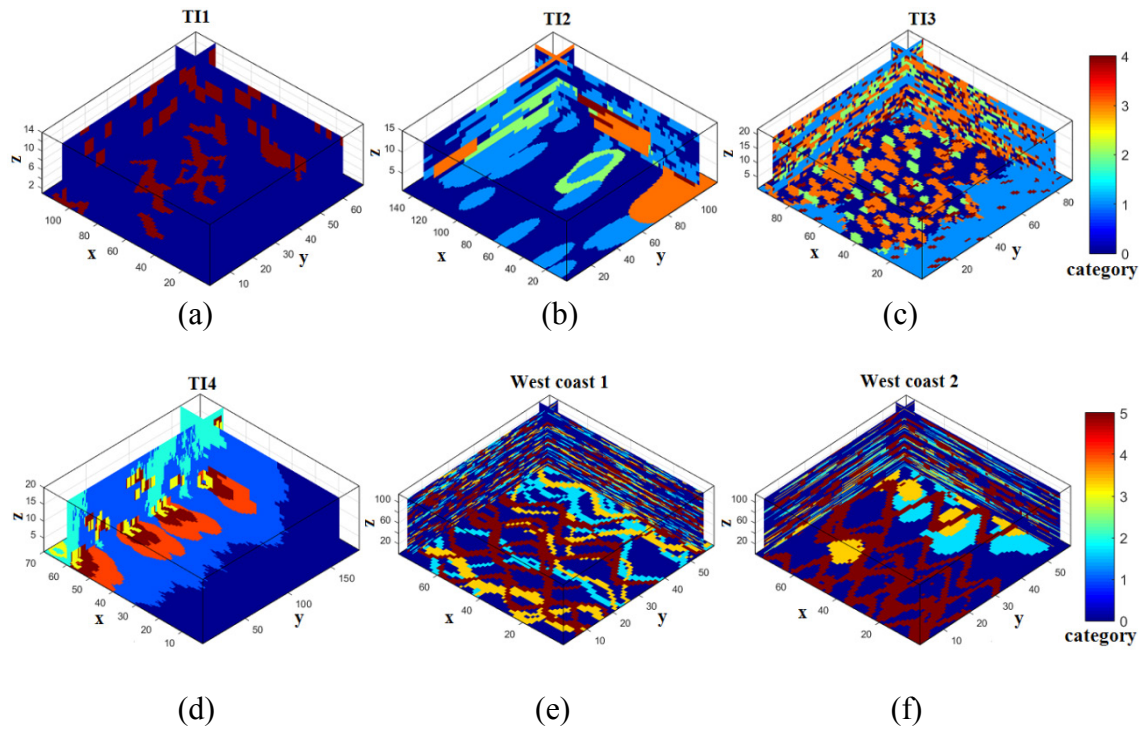


Figure 4.1: Six 3D Models

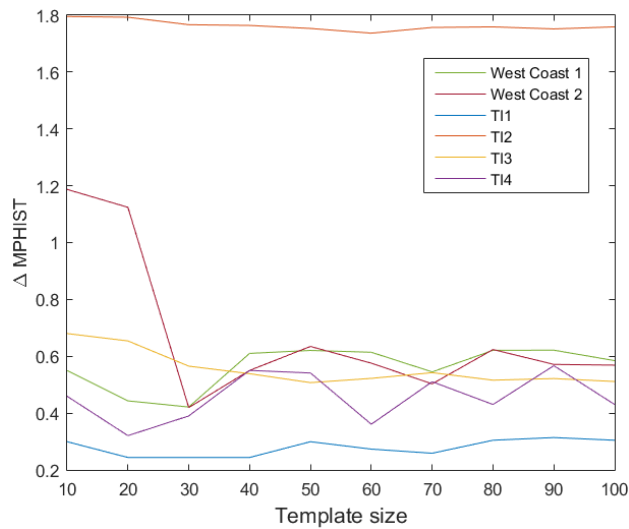


Figure 4.2: Comparing $\Delta MPHIST$ of 10 different template sizes

Unconditional realizations are compared with $\Delta MPHIST$ in Figure 4.2. It can be seen from the Figure 4.2 except for the TI1, which is very stationary, that the $\Delta MPHIST$ results (based on template size $2 \times 2 \times 2$) decrease as the template size getting large. However, it also

indicates that a larger template not necessarily generates better results with lower Δ MPHIST. The downward trend turns flat after the size of 50-point template. The optimal template for 3D TIs should be larger than 50 points.

The first three rows in Table 4.1 are randomly selected conditional realizations from the three data spacings. Data spacing 10×10 is the densest drilling, while 30×30 is the sparsest. The realizations show the same slices as the corresponding TIs in Figure 4.1 show. It can be seen from the second row (TI2) and the fourth row (TI4) that as the number of samplings decreases to unconditional, the quality of the realizations is clearly reduced. The features in the unconditional realizations have unclear boundaries and the shapes are changed. However, there are few differences between conditional realizations and unconditional realizations for rest of the TIs. The reason is that TI determines the main features of realizations, unless the hard data are numerous. Hence, if there is a lot of sample data, the structures they reveal, especially medium to large structures, prevail over the structures read from the TI and result in poor replication of the TI (Strebelle, 2002).

Table 4.1 (a): Conditional realizations with different data spacing and unconditional realizations

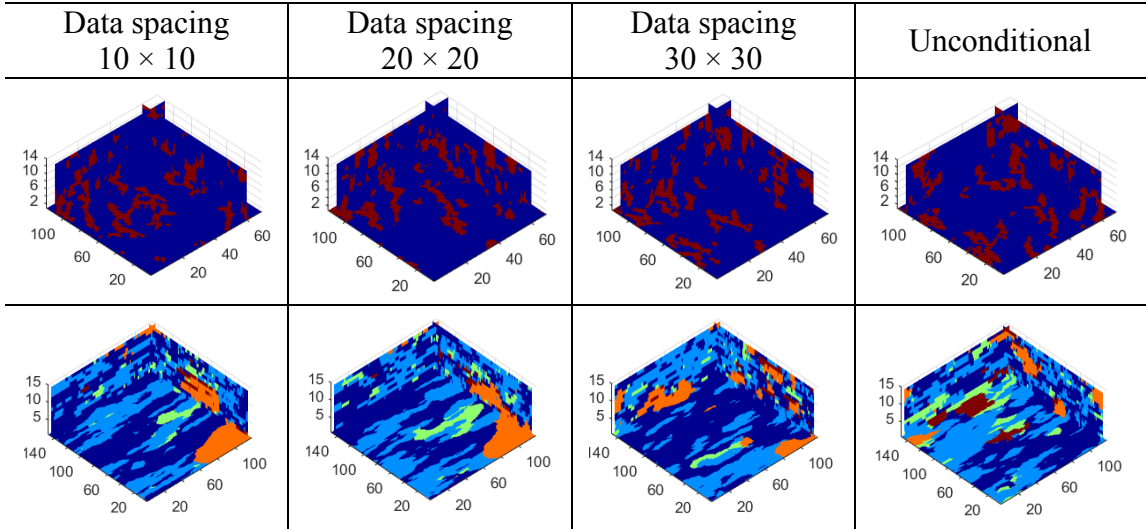


Table 4.1 (b): Conditional realizations with different data spacing and unconditional realizations

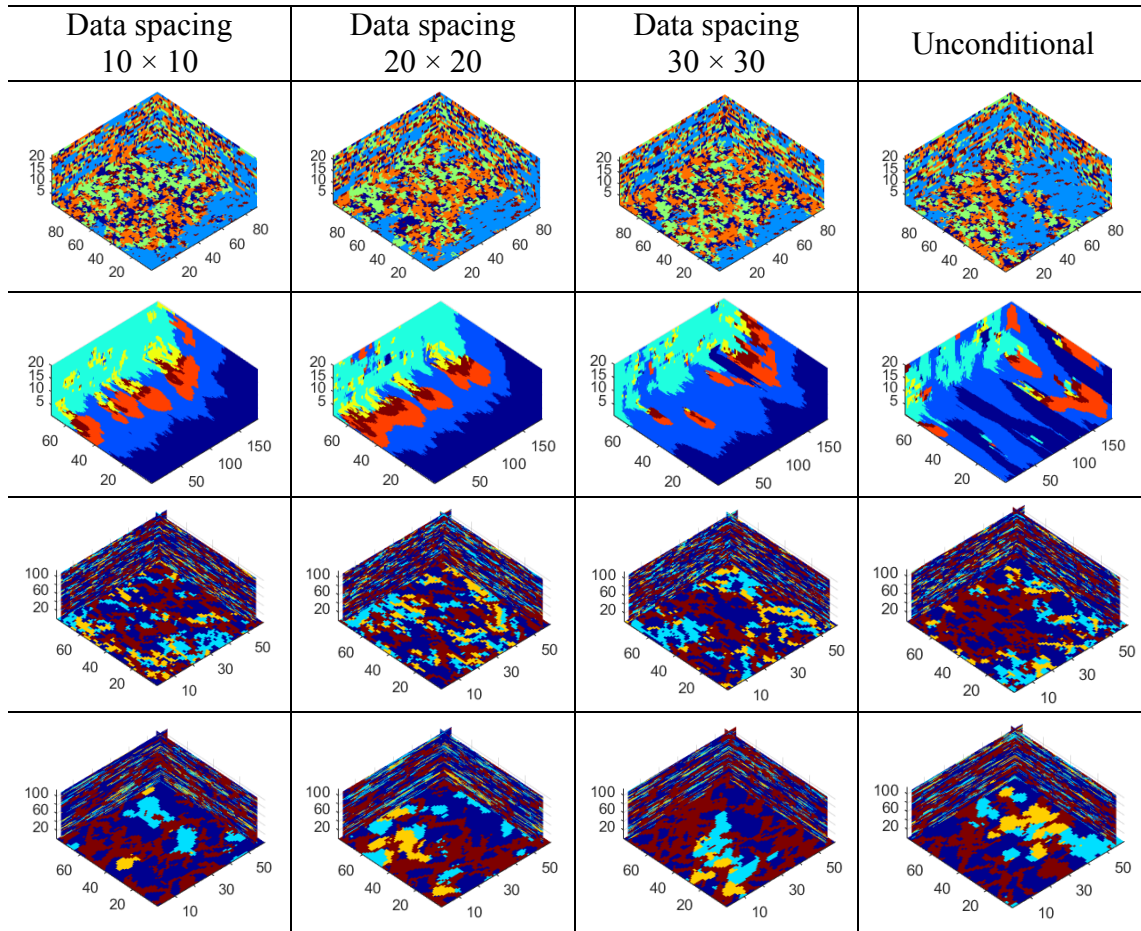


Figure 4.3 presents the mean of Δ MPHIST results of the realizations shown in Table 4.1. Figure 4.3 (a) compares the original SNESIM results, and Figure 4.3 (b) is comparing the SNESIM 4.0 results (Strebelle, 2014). In Figure 4.3 (a), the Δ MPHIST of TI2, TI3, and TI4 increases clearly as the amount of drillings decreases, which are the same results as the realizations show in Table 4.1. In addition, TI1 and the west coast data show more flat and even opposite Δ MPHIST results that are similar to the quality of the realizations. The Δ MPHIST of TI1 barely changes when the amount of conditioning data decreases; the Δ MPHIST for west data increases a little when drillings are getting fewer, and drops where

it is unconditional simulation. Δ MPHIST results match with visual results again that proves the reliability of using Δ MPHIST to assess the realizations are reliable.

Simulation results are affected by another parameter, the “maximum number of conditioning data.” The bigger this parameter’s number, the more conditioning data can be used. Through numerous tests, when there is more conditioning data, it takes longer to retrieve the conditional probability from the search tree as. However, a different “maximum number of conditioning data” results in the same trend of Δ MPHIST results as shown in Figure 4.3. This parameter can be decided by an experimental number is 16, and it does not affect sensitivity test results.

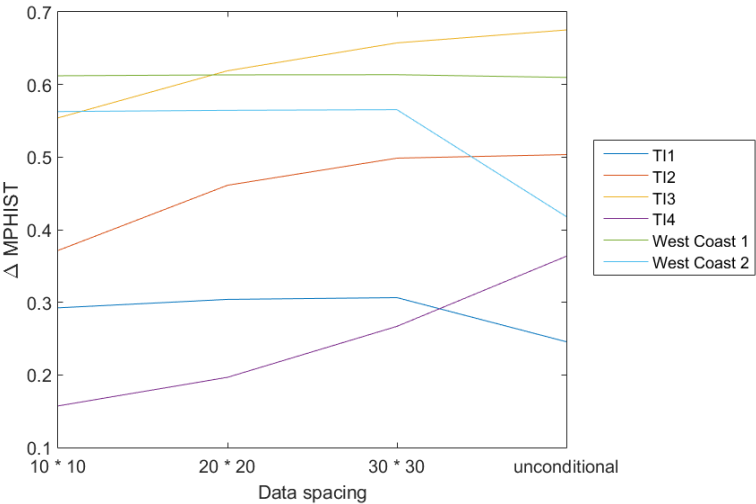


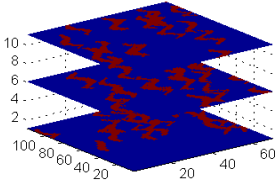
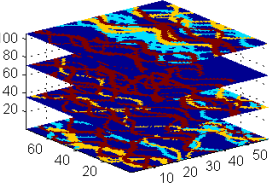
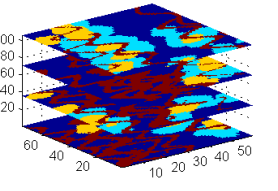
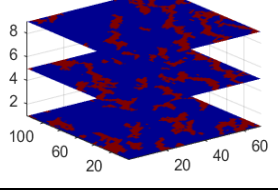
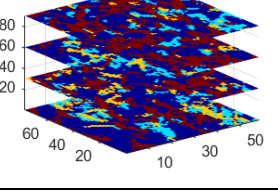
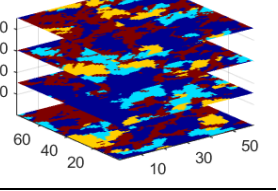
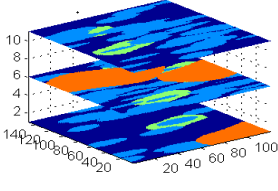
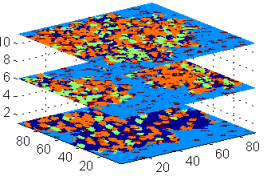
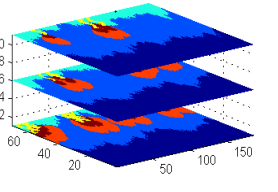
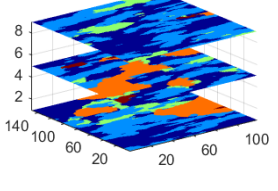
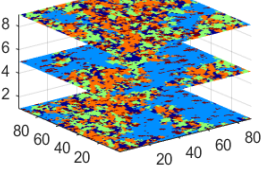
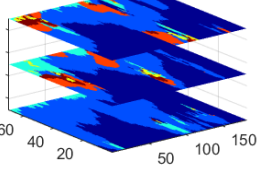
Figure 4.3: Δ MPHIST for three-data spacing and unconditional realizations

4.1.2 Stationarity Assessment

The performance of MPS simulation depends not only on parameter settings, but also the TI itself. This section focuses on the quality of the realizations and relates the quality to TI stationarity. Statistical results of stationarity test from Chapter 2 are shown in Table 4.2. With the unconditional realizations presented in row 2, the final stationary levels for 3D TIs are determined at the bottom row. The #2 and #3 are fluvial TIs but not stationary as the

T11, because their statistical results are uncertain and the unconditional realizations both have average qualities. The other three TIs have similar stationarity testing results both in statistically and visually, they are easily determined to be medium or poor stationary.

Table 4.2: Evaluate stationarity by statistics and unconditional simulation performance

# of TI	1	2	3
TIs			
Unconditionl realizations			
Category Distribution	0.77	0.77	0.5
MPHIST	0.08	0.03	0.08
Stationarity level	Good	Good	Good
# of TI	4	5	6
TIs			
Unconditionl realizations			
Category Distribution	0.55	0.46	0.1
MPHIST	0.57	0.1	16.3
Stationarity level	Medium	Medium	Poor

The exact cut-offs for differentiating stationarity levels are given in Table 4.3. Cut-offs are determined on the value of the last TI belonging to that stationarity level group, the same method as it was introduced in Chapter 3.

Table 4.3: Cut-offs for stationarity level

Methods	Category distribution	MPHIST
Good	> 0.5	< 0.08
Medium	0.1-0.5	0.08-16.3
Poor	< 0.1	> 16.3

4.2 Large Number of Rock Types TI Example

4.2.1 Background of the Copper TI

In this section, conclusions drawn from previous TIs are employed to analyze a large copper-style TI with 15 irregular shaped rock types. This case study is referred to the work of Verly et al., (2009). The research area was obtained from a deep and sparsely drilled deposit, the Resolution porphyry-style Cu-Mo deposit in Arizona, United States. The age of the deposit is late-Cretaceous to early Tertiary and is hosted within a buried, fault-bounded sequence of Paleozoic and Precambrian sedimentary strata, Precambrian diabase sills and Cretaceous-aged layered volcanoclastic and siliciclastic rocks. The geological formation is complex, containing faults, intrusions, breccias, metamorphosed rocks of sedimentary origin. The TI has dimension of 108×140×64 cells, constituted by 15 categories; conditioning data used in simulation are shown in Figure 4.4.

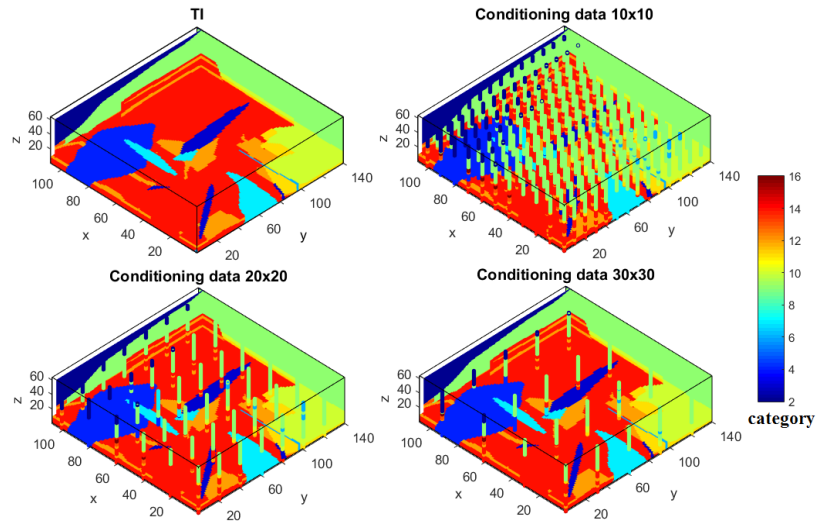


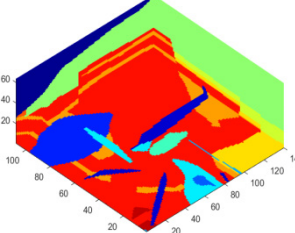
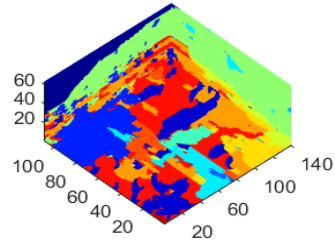
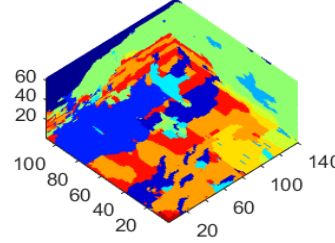
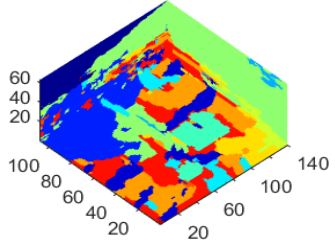
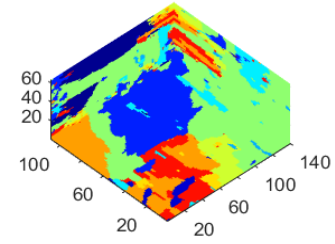
Figure 4.4: Porphyry model and drillings for conditional simulation

4.2.2 Simulation of the Large Copper TI

Tested with the categorical distribution, the large copper TI has a result of 0, which is not surprising because of its complexity with too many categories. According to the optimal selection summarized previously, simulation is employed with a template with 60-point, on 5 multi-grid, and the searching ellipse is set to similar to the dimension of the TI.

Table 4.4 compares the conditional realizations to unconditional realization. The results of Δ MPHIST are based on the 2×3 template size. It can be seen from the statistics that as the number of conditioning data decreases, the Δ MPHIST increases. At the same time, the quality of the realizations shows the missing features from dense drilling to unconditional situation. For example, the realization from the densest drilling even reproduces the little dark blue intrusions inside the triangle light blue, none of the other realizations do that; the unconditional realization accurately replicates few features. This table indicates the reliability of using Δ MPHIST to assess the realizations.

Table 4.4: Conditional realizations with three data spaces and unconditional realizations

TI	10×10 [0.31]	20×20 [0.36]
		
	30×30 [0.38]	Unconditional [0.43]
		

4.3 Discussions

Seven 3D TIs have been assessed for “goodness” of generating realizations in this chapter. The first rule is summarized through sensitivity tests of six simpler 3D TIs. It has been found that template size can be fewer when the TI is very stationary, if similar to the TI1, which has good stationarity scores and well-behaved unconditional realizations. The three non-channel TIs with medium to poor stationarity show more reliance on conditioning data when simulating. The denser the sample data are, the more accurate the replications of the features from the TI. However, some issues about using conditioning data are: (1) the data need to conform to the TI, which might not be realistic in the real life; (2) the dense conditioning data can reduce the replications of medium-to-large-scale structures that appear in the fluvial-type TIs.

The case study for the copper TI with 15 rock types is challenging, since the TI contains many rock types and is highly unstationary. It is difficult to create accurate shape

reproduction without the control of the conditioning data. MPS simulation is applied to look for better a solution for geological modeling of similar deposits. The geological setting of the TI will be used in Chapter 5, to apply a hierarchical approach for improving the reproduction in simulation.

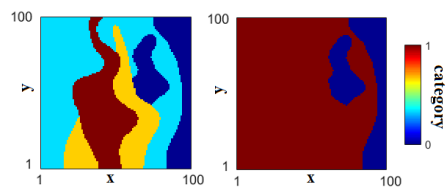
Finally, through the application of MPS simulation, it can be found that the stationarity does affect the selection of the parameters and the quality of the realizations. To perform realizations assessment, Δ MPHIST is solid to employ.

Chapter 5

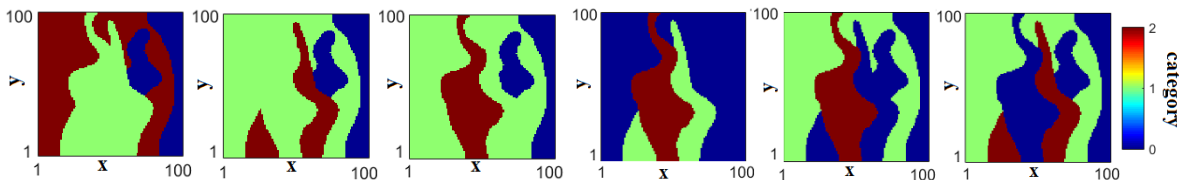
Hierarchical Simulation

5.1 Hierarchical Simulation Methodology

MPS simulation reproduces features from the TI in the realizations. However, as the number of categories increases, the difficulty of accurately replicating these features increases. One methodology to help counter this disadvantage is hierarchical MPS simulation. The idea is to re-code and lump categories based on geological or graphic features, and simulate with the new model in a step-wise fashion considering only a few categories in each step. An example of different lumping in every step of hierarchical simulation is shown in Figure 5.1 (b) and Figure 5.1 (c). Figure 5.1 (a) shows the first step in lumping by modifying the TI into binary pattern, Figure (b) and (c) shows the possible lumpings in step two and three. Figure 5.1 (d) is another possible lumping of categories (3 and 4) in the first step, and (e) is the modified TI in second step. The workflow for hierarchical simulation procedure is presented in Appendix B.



(a)



(b)

(c)

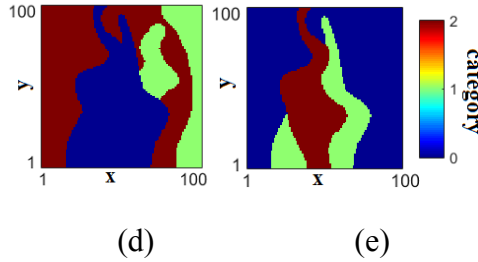


Figure 5.1: Some lumpings of the porphyry TI: (a) TI and an one of the modified binary patterns; (b) TIs (based on the pattern in the first step) in the second step; (c) TIs in the third step; (d) another ordering of merging 2 categories in the first step; (e) TI in the second step

Many previous works have shown the advantages of the hierarchical approach and have been discussed in Chapter 1. Here, six 2D TIs with more than 2 categories are implemented with all the possible lumpings in a hierarchical simulation using SNESIM. Optimal lumping orderings are quantified and rules for combining categories are determined to help in the selection of which categories to merge. Realization quality is quantified through visual inspection and statistical comparison using MPHIST.

5.2 Statistical Relationships for Assessing TIs

In order to analyze TIs and to summarize rules for hierarchical simulation, the statistical relationships for categories are calculated here, using three types of assessments: the distance matrix, the contact area matrix, and the transition matrix. Distance matrices compute the shortest distance between pairs of categories for each cell in the TI. Contact area matrices calculate the shared area between two contacting categories in the TI. The transition probability matrix indicates if the category is connected to nearby categories. Each row sums to 1.0.

The goal is to determine, based on these statistics, which categories should or should not be merged. Realizations of different orderings are checked for ΔMPHIT , in order to assess how ordering influences the final realizations. In addition, statistical relationships and visual inspection of realizations are also important criteria to assess and summarize ordering rules. The goal is to determine rules based on the features of the TI to help determine which categories should be merged. The details of the programs used to calculate the related statistics are given in Appendix.

5.2.1 Distance between Categories

Calculating the minimum distance between categories in a TI may suggest which categories should not be simulated together in hierarchical simulation. Figure 5.3 is an example of the shortest distance between pairs of categories. In this chart, d_{31} , d_{21} , and d_{23} are shortest distance from E_3 to E_1 , E_2 to E_1 , and E_2 to E_3 .

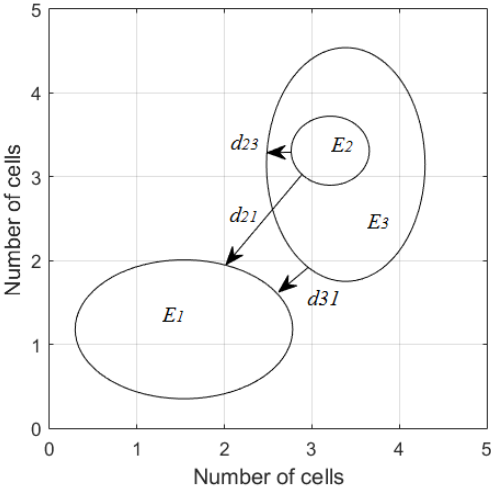


Figure 5.2: An example of the shortest distance between two categories

The $K \times K$ matrix of the closest categories is calculated, where K is the number of categories. Figure 5.2 is a TI with 5 categories used to demonstrate how this and other two statistical relationships work.

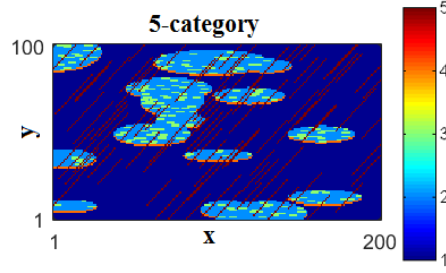


Figure 5.3: A 5-category TI (Lyster et al., 2004).

The matrix below is the distance matrix computation and is not symmetric. The distance from category 1 to category 4 is different when computing it inversely. Green values show categories that are close, while red values are categories that are far from each other. Table 5.1 indicates that category 1 is close to category 4, category 2 is close to category 4, while 3 is far from category 1.

Table 5.1: Distance between pairs of categories

	1	2	3	4	5
1	-	10.99	12.73	12.49	3.80
2	4.30	-	2.21	6.26	3.20
3	4.54	1.05	-	5.93	3.25
4	1.04	1.19	3.04	-	3.55
5	1.63	7.90	9.74	10.30	-

5.2.2 Contact Area

Figure 5.4 is an example of several types of categorical contact relationships. In 2D, contact area is calculated in the form of the perimeter. Denote the area of ellipses E_1, E_2, E_3 , as A_1, A_2, A_3 and A_4 . Contacts between ellipses are highlighted in red as C_{12}, C_{34} . E_1 is completely contained in E_2 , hence the contact area for E_1 to E_2 is 1, and E_2 to E_1 equals to C_{12}/A_2 . The contact area of E_3 to E_4 is calculated by C_{34}/A_3 , and E_4 to E_3 is C_{34}/A_4 .

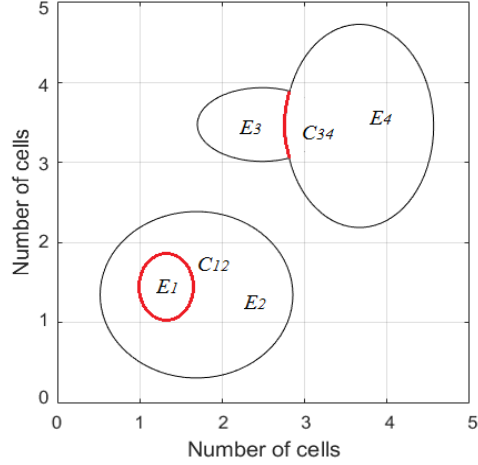


Figure 5.4: An example of contact relationship

The contact area is shown in Table 5.2, green values indicate categories sharing a large contact area, while red values mean they barely contact. It can be found that category 1 is the least related to the inclusive category 3, since the “3” is included in category 2. Due to the unique shape of category 4, it shares little area with other 4 categories.

Table 5.2: Contact area for pairs of categories

	1	2	3	4	5
1	-	0.07	0.01	0.08	0.84
2	0.11	-	0.41	0.10	0.38
3	0.03	0.77	-	0.05	0.15
4	0.44	0.32	0.08	-	0.16
5	0.73	0.20	0.04	0.03	-

5.2.3 Transition Probability Matrix

By composing a string of data with length of \mathbf{h} , the probability of transitioning category i to category j :

$$t_{ij}(\mathbf{h}) = \Pr\{I_i(\mathbf{u}) = 1, I_j(\mathbf{u} + \mathbf{h}) = 1\} \tag{Equation 5.1}$$

Where \mathbf{u} is the starting location, \mathbf{h} is the length between two categories. The transition probability matrix for all K categories is defined as:

$$T(\mathbf{h}) = \begin{bmatrix} t_{11}(\mathbf{h}) & \cdots & t_{1K}(\mathbf{h}) \\ \vdots & \ddots & \vdots \\ t_{K1}(\mathbf{h}) & \cdots & t_{KK}(\mathbf{h}) \end{bmatrix} \quad \text{Equation 5.2}$$

The higher the transition probability $t_{ij}(\mathbf{h})$ is, the higher chance that category i will transition to category j at a distance of \mathbf{h} , and i and j should be close to each other. Figure 5.5 is an example of how the transition probability works.

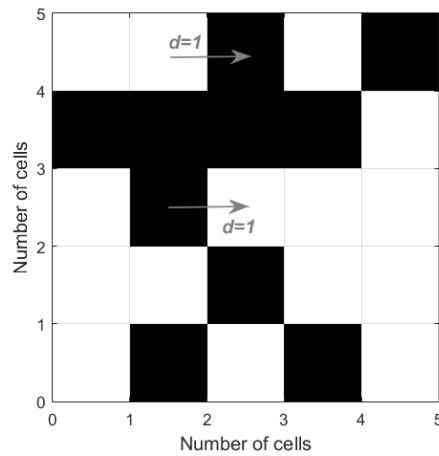


Figure 5.5: An example of transition probability computation (the arrow indicates the direction of the transition, distance d is given as 1)

Table 5.3 demonstrates transition probabilities between pairs of categories. Category 5 has a greatest chance to be transformed to category 1, but category 1 is not ideal to be transformed to category 2, 3 or 4.

Table 5.3: Transition probability for pairs of categories

	1	2	3	4	5
1	0.9042	0.0041	0.0004	0.0034	0.0878
2	0.0161	0.8437	0.0371	0.0082	0.0949
3	0.0069	0.1482	0.7597	0.0074	0.0778
4	0.1168	0.0723	0.0165	0.6904	0.1041
5	0.6799	0.1899	0.039	0.0235	0.0677

2D TIs are used to generate realizations with hierarchical simulation with all possible sequences of merging of categories, and the realizations are compared using Δ MPHIST. The qualities of the realizations and the statistical relationships between categories are both important criteria to assess how different ordering influences simulation, and how to decide the rules based on features of the TI to help guide practitioners wanting to use MPS with many categories.

5.3 Hierarchical Rule Definition

5.3.1 TIs with Three Categories

The complexity of hierarchical simulation depends on the number of categories in the TI. The simplest situation is with 3 categories (Figure 5.6). In the first step, TIs are modified to be binary, which is two categories combined together as background, while the other category is simulated. In the second step, the simulated category is frozen. The final realization is assembled by recovering modified codes from the last step. Simulations are applied in a modified SNESIM program which is given in Appendix.

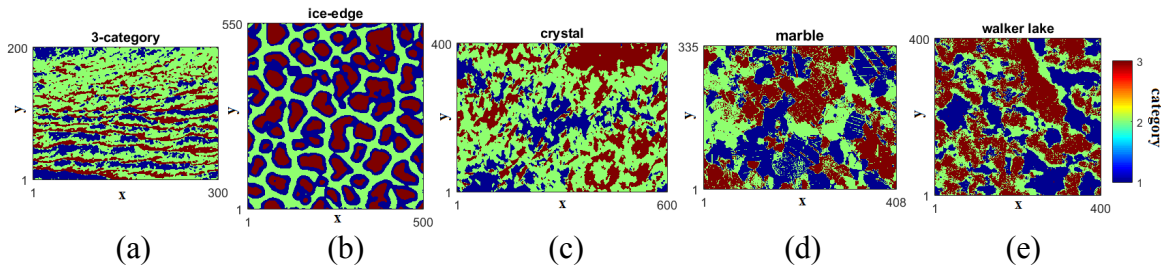


Figure 5.6: TIs with only 3 categories: (a) 3-category TI; (b) ice-edge solid TI; (c) crystal TI; (d) thing marble TI; (e) Walker lake TI.

Figure 5.7 shows the Δ MPHIST (based on 2×2 template) of 5 TIs for all possible orderings, showing the importance of selecting the correct/best ordering. The best and worst orderings

that are measured through the value of ΔMPHIST are presented in Table 5.4. Selected realizations for traditional unconditional simulation are included for comparison. The best ordering for crystal, marble and Walker Lake TI is the second ordering “2,13”, which stands for simulating the second category alone in the first step. Two other TIs, the ice-edge and 3-category TI show more flat results when altering the ordering, and the best lumping both occur at the third one, which is merging the category 1 and 2 together.

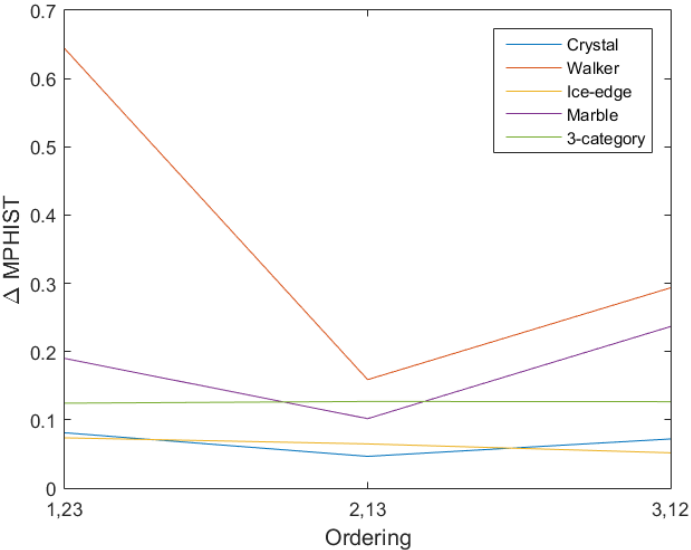
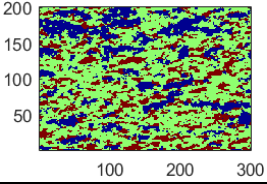
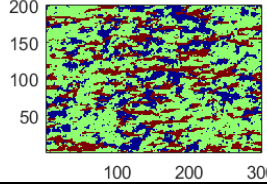
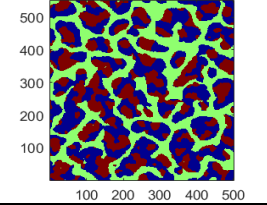
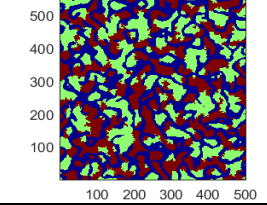
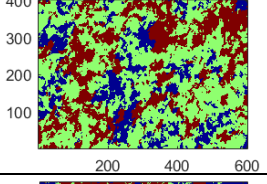
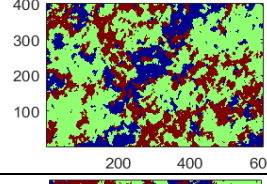
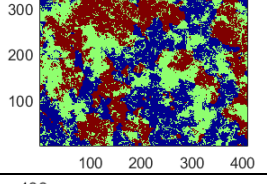
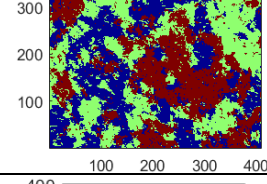
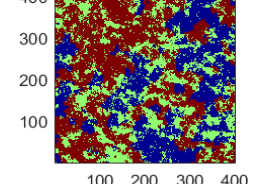
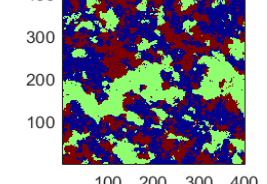


Figure 5.7: Testing ΔMPHIST results of all 6 possible orderings

In Table 5.4, realizations from the (minimum ΔMPHIST) and the worst ordering (maximum ΔMPHIST), with the corresponding ordering, are compared to prove the validity of statistical results. It can be seen, especially from the second row and the last row that features are replicated more accurately when applying the good ordering than the poor ordering. 3-category does not show many differences even on the realizations, which matches with the ΔMPHIST results. However, wrong lumping renders worse realization the standard simulation.

To determine rules of how to predict optimal ordering, the statistical relationships between categories in the TI are assessed and compared to the optimal ordering determined from Figure 5.7. Three types of statistical relationships are presented in Table 5.5, Table 5.6 and Table 5.7.

Table 5.4: The minimum and maximum Δ MPHIST realizations for different orderings

Good Realizations	Min Δ MPHIST (Temp size 2×2)	Poor Realizations	Max Δ MPHIST (Temp size 2×2)
	1,23 [0.11]		2,13 [0.13]
	3,12 [0.05]		1,23 [0.09]
	2,13 [0.04]		1,23 [0.09]
	2,13 [0.09]		3,12 [0.26]
	1,02 [0.14]		0,12 [0.65]

For ice-edge TI, the best ordering occur at combining category 1 and 2, which matches with its statistical relationship shown in all of the three Tables that category 1 and 2 share large contact area, close distance and high transition probability. 3-category TI does not

show too many differences, but statistics matches with simulation results that category 2 and 3 merged together. For marble, crystal and Walker lake TI, both of the best ordering at combining category 1 and 3 (category 0 and 2), but these two categories are not closely related. Because the other category has a great connection with category 1 and 3 (category 0 and 2), to merge 1 and 3 in the first step and simulate with two closer relations instead of simulating two disconnected categories at the same time which improve the quality of the image. The reason of different results is that the ice-edge the best merging for ice-edge TI creating an image that is stationary and easy to be reproduced as well. Whether categories share close relationship or distinct relationship should be merged needs more discussion in the following content.

Table 5.5: Contact area (red is not so related, green is closely related)

3-category	1	2	3	Ice-edge	1	2	3	Crystal	1	2	3	Marble	1	2	3	Walker lake	0	1	2
1	-	0.90	0.10	1	-	0.55	0.45	1	-	0.98	0.02	1	-	0.98	0.02	0	-	0.78	0.22
2	0.43	-	0.57	2	1.00	-	0.00	2	0.38	-	0.62	2	0.42	-	0.58	1	0.24	-	0.76
3	0.08	0.92	-	3	1.00	0.00	-	3	0.01	0.99	-	3	0.02	0.98	-	2	0.08	0.92	-

Table 5.6: Distance between categories

3-category	1	2	3	Ice-edge	1	2	3	Crystal	1	2	3	Marble	1	2	3	Walker lake	0	1	2
1	-	2.09	5.67	1	-	6.32	6.13	1	-	4.08	10.61	1	-	3.50	7.76	0	-	4.80	6.37
2	4.36	-	3.44	2	4.74	-	14.15	2	14.28	-	5.80	2	6.03	-	4.70	1	5.08	-	2.66
3	5.07	1.55	-	3	6.07	15.80	-	3	26.21	5.06	-	3	9.86	2.77	-	2	11.32	2.59	-

Table 5.7: Transition probability matrix

3-category	1	2	3	Ice-edge	1	2	3	Crystal	1	2	3	Marble	1	2	3	Walker lake	0	1	2
1	0.87	0.12	0.01	1	0.94	0.03	0.03	1	0.91	0.08	0	1	0.91	0.09	0	0	0.92	0.06	0.02
2	0.05	0.9	0.05	2	0.04	0.96	0	2	0.03	0.92	0.05	2	0.09	0.79	0.12	1	0.06	0.74	0.20
3	0.01	0.12	0.87	3	0.04	0	0.96	3	0	0.08	0.92	3	0	0.13	0.87	2	0.01	0.14	0.85

5.3.2 TIs with More Than Three Categories

With more than 3 categories, TIs are employed with a more complicated ordering by modifying more than 1 category at a time. The stationarity of these TIs were assessed in

Chapter 2 and Chapter 3. Two TIs are implemented with every possible merging. The porphyry TI with four categories has 18 orderings, and the 5-category TI has 100 orderings.

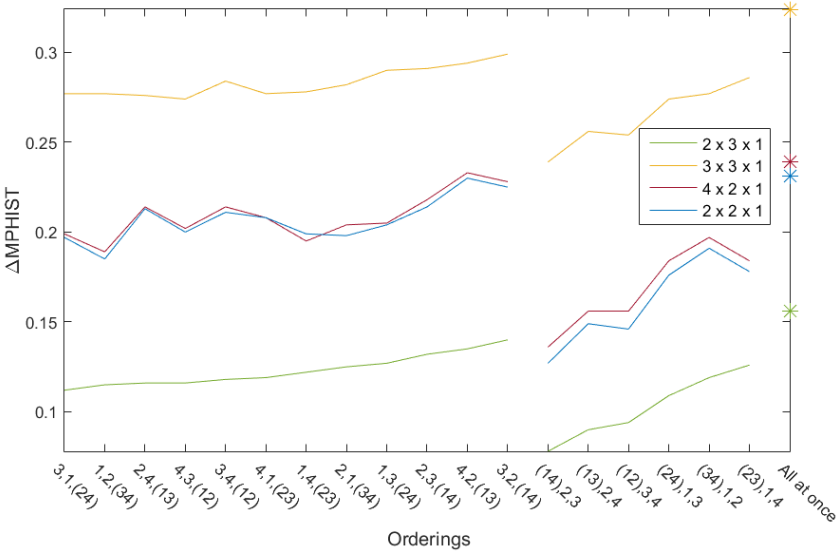
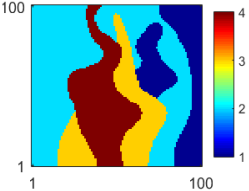
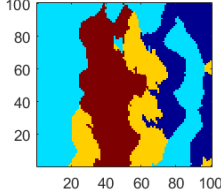
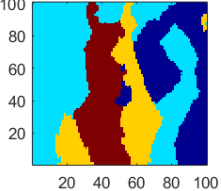
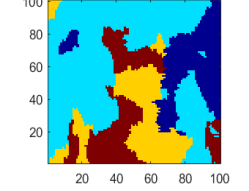
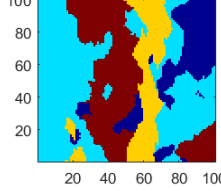
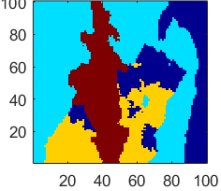


Figure 5.8: Comparing Δ MPHIST of realizations from 18 orderings for the porphyry TI in hierarchical simulations to the traditional simulation that simulates all categories simultaneously

Figure 5.8 compares all 18 possible orderings in hierarchical simulation with the traditional simulation that simulates all simultaneously. There are two parts in the figure that represent the result of Δ MPHIST from two different types of lumping. The first part before lines break is merging 3 categories in the first step, lumping only one category in each step; the second part is merging 2 categories in the first step, while 2 others left unchanged; the third part is the standard MPS simulation. The details of three lumping types are provided in Appendix. Results are sorted based on the results of the 2x2 template. Other similar plots in this chapter follow the same format. It can be seen in Figure 5.8 that hierarchical simulation generates better realizations with lower Δ MPHIST than standard MPS simulation; having more categories merged in the first step decreases the value of Δ MPHIST.

Table 5.8 shows realizations with minimum ΔMPHIST (the best ordering) and maximum ΔMPHIST (the worst ordering) in hierarchical simulation and simulating all at once. The best ordering 3,1,(24) of the first part in Figure 5.8 replicates more specific features from the TI than the ordering the worst 3,2,(14). When merging two categories in the first step, the best ordering of merging rock type 1 and 4, while simulating the 2 and 3 renders the lowest ΔMPHIST .

Table 5.8: Realizations

TI Porphyry	Min ΔMPHIST (temp size 2×2)	Method #1 3,1,(24) [0.18]	Method #2 (14),2,3 [0.13]
			
All at once [0.25]	Max ΔMPHIST (temp size 2×2)	3,2,(14) [0.23]	(34),1,2 [0.19]
			

Method #2 shows that 1 and four makes the best combination is that category 1 and 4 are not touched, they are lumped and then frozen in the second step, which allows for the rest of the closely connected categories to be simulated together. It also found in the method #1 that when simulating category 1 and 4 together in the last step, the realizations are the worst. The second best ordering in Figure 5.8 is 1,2,(34), which means to simulate category 3 and 4 that are two categories sharing large contact area together. This case study prefers that two closely related categories should be simulated not merged together. Moreover, hierarchical simulation shows better feature reproduction than simulating all categories at once.

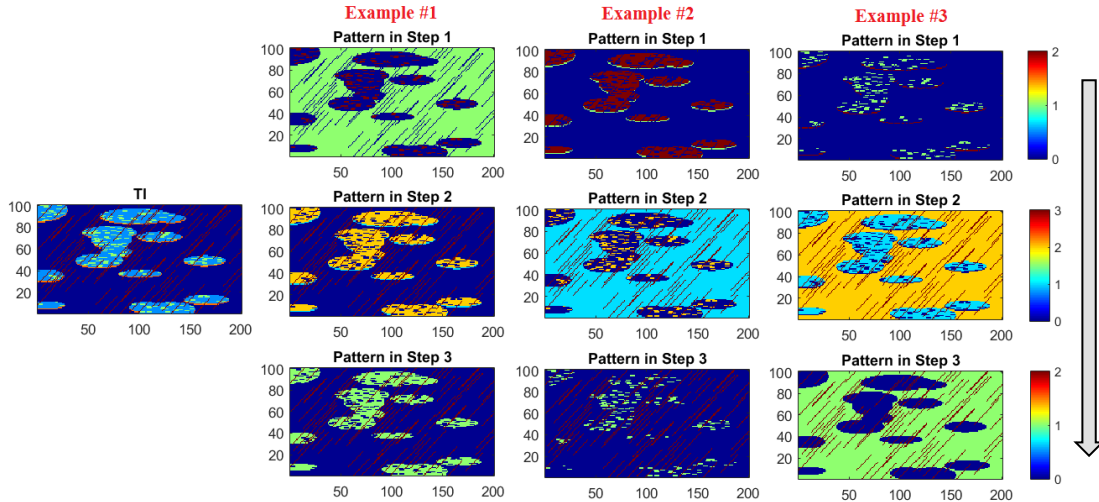


Figure 5.9: Examples of merged patterns in every step (arrow indicates the sequence)

The 5-category TI shows a lot of complexity when analyzing all possible combinations. The total number of all possible orderings for hierarchical simulation is 100. There are 60 non-repetitive groups of simulating each single category during every step, 30 for combining 3 categories in the first step, and 10 for merging 2 out of 5 categories in the first step. In addition to the amount of groups, the features of categories themselves are intricate, which increases the difficulty of ideal shape replication. Because there is one more category in this TI than the porphyry TI, another type of lumping is applied to this TI. The details are provided in Appendix. Figure 5.9 demonstrates three examples (out of 30) of the patterns in every step of simulation of this type of lumping, which corresponds to the second part of Figure 5.10.

Figure 5.10 compares Δ MPHIST results of three types of lumping in hierarchical simulation and standard MPS simulation. First part before lines break is constituted of 60 orderings of simulating one category during each step. Second part is constituted of 30 orderings that is demonstrated in Figure 5.9. Three steps are needed in this type of lumping.

The third part comprises 10 orderings of merging two categories in the first step, which requires only two steps to finish simulation.

One conclusion is that fewer steps of simulation return lower median value of ΔMPHIST . Standard simulation has lower ΔMPHIST than some of the orderings, indicating that wrong lumping can perform worse than standard simulation. The best ordering for the first part is simulating category 5 that are slashes, a distinctive shape, in the first step. The other two methods are discussed with Table 5.9.

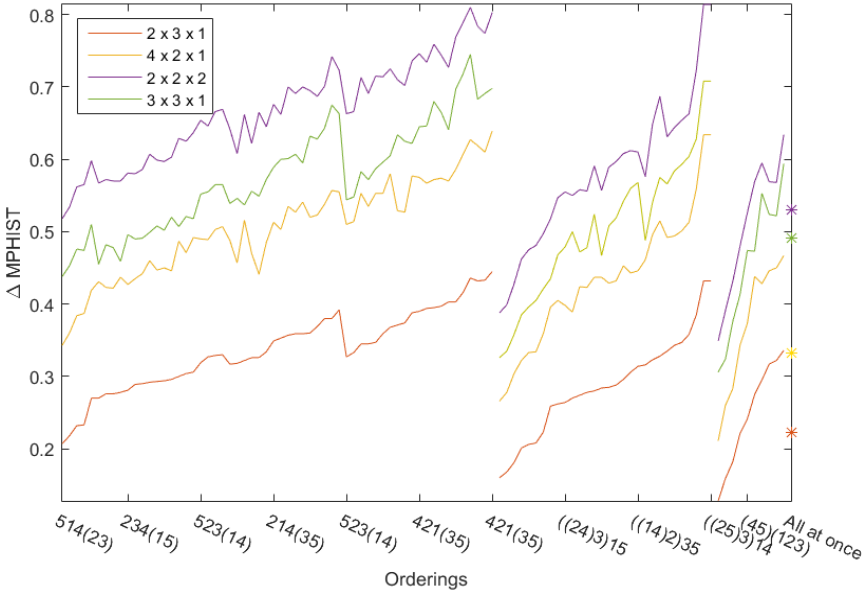
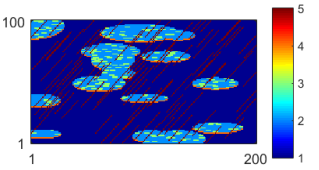
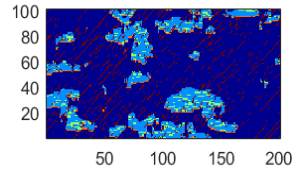
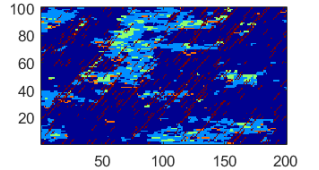
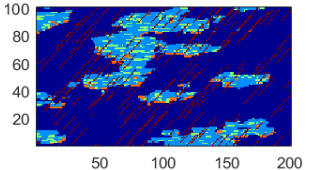
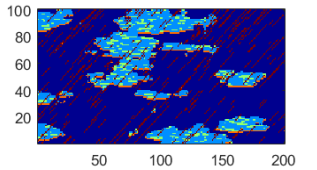
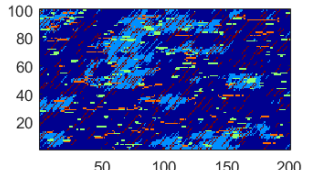
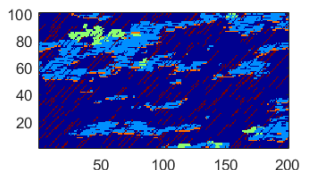
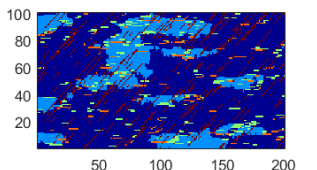


Figure 5.10: Comparing ΔMPHIST of realizations from 100 orderings in hierarchical simulations to the traditional simulation that simulates all categories at the same time

Table 5.9 compares realizations of good and poor orderings from hierarchical simulation. Visually, the worst realizations have some of the features dislocated, producing fewer than the good realizations, even standard MPS simulation shows better feature reproductions than the poor realizations in hierarchical simulation. The statistics for this TI is presented in section 5.2. In method #1, category 2 and 3 left in the last step have large contact area and result in a TI that is more stationary thus has a lower ΔMPHIST . The best

ordering in method #2 is (15) 4 (23), which is simulating category 1 and 5 in the first step and other categories are merged. The best ordering in third method is (145) (23), which means to merge category 2 and 3 in the first step, and to simulate them in the second step. Since category 1 and 5, 2 and 3 both share large contact area, close distance, and high transition probability, they should be simulated together during simulation in order to generate the Min Δ MPHIST. However, since 3 is completely contained in 2, it is not wrong to merge them.

Table 5.9: Comparing realizations of hierarchical simulation and traditional simulation

TI 5-category		All at once [0.23]	
Min Δ MPHIST (temp size 2×2)	Method #1 514(23) [0.19]	Method #2 (15)4(23) [0.16]	Method #3 (145)(23) [0.11]
			
Max Δ MPHIST (temp size 2×2)	431(25) [0.48]	(25)3(14) [0.44]	(134)(25) [0.36]
			

The rules for hierarchical simulation are:

1. Categories that share large contact areas should be considered as a group. If one is contained in another category, they can be merged in first steps; or if they are not similar, they should be simulated together in the last step.

2. From the example of 5-category TI, the most isolated category should be simulated at first. Therefore it will be frozen for the rest of the steps.
3. From the examples in section 5.3.1 that categories share few connections need to be merged to improve the quality of the TI.
4. Categorical relationships do help predict what type of lumping works for the TI.

5.4 3D TIs

5.4.1 3D TIs with Fewer than 6 Categories

Constructing realizations with all possible orderings for 3D TIs is time consuming, therefore only the two 3D models with five categories are assessed with all possible orderings, to further discuss if the rules summarized in the previous section work for 3D TIs. TI4 is employed with 15 orderings, to check if rules. TIs are shown in Figure 5.11, and the details have been introduced in Chapter 2.

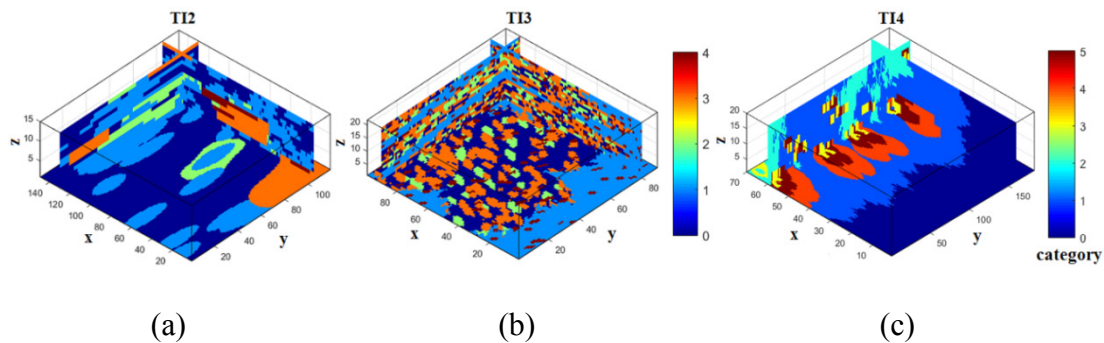


Figure 5.11: 3D TIs

According to the rules determined with 2D TIs, the first step to decide the ideal ordering is to calculate the relationship between categories. Table 5.10, Table 5.11 and Table 5.12 present distance, contact area, and transition matrix between each pair of categories. The statistics between two categories indicate which two categories should be concerned first.

However, other combinations are also considered in order to explore the correctness of the rules. For the first TI, categories 0 and 1 show a major containment, so they need to be simulated together.

Table 5.10: Statistical relationships for TI2 (green means closely related, red means not so close)

Tidal-dominated	Contact area					Distance					Transition matrix				
	0	1	2	3	4	0	1	2	3	4	0	1	2	3	4
0	-	0.79	0.10	0.07	0.04	-	1.76	7.81	12.67	15.64	-	0.07	0.01	0.00	0.00
1	0.75	-	0.16	0.05	0.04	1.52	-	6.37	12.35	13.91	0.08	-	0.02	0.00	0.00
2	0.34	0.59	-	0.04	0.03	1.77	1.53	-	12.46	14.62	0.05	0.10	-	0.01	0.00
3	0.35	0.28	0.06	-	0.32	2.39	2.31	6.29	-	9.87	0.01	0.01	0.00	-	0.01
4	0.28	0.26	0.06	0.41	-	2.11	1.87	5.80	4.41	-	0.01	0.01	0.00	0.02	-

Table 5.11: Statistical relationships for TI3 carbonate

Carbonate	Contact area					Distance					Transition matrix				
	0	1	2	3	4	0	1	2	3	4	0	1	2	3	4
0	-	0.12	0.28	0.47	0.13	-	0.03	0.11	0.16	0.06	-	0.02	0.02	0.00	0.00
1	0.17	-	0.14	0.28	0.41	0.01	-	0.01	0.02	0.06	0.02	-	0.01	0.00	0.01
2	0.35	0.12	-	0.38	0.15	0.13	0.03	-	0.08	0.06	0.05	0.05	-	0.02	0.00
3	0.40	0.16	0.27	-	0.18	0.11	0.03	0.05	-	0.06	0.04	0.02	0.08	-	0.01
4	0.18	0.38	0.16	0.28	-	0.10	0.22	0.09	0.16	-	0.00	0.06	0.00	0.00	-

Table 5.12: Statistical relationships for TI4 fluvial-deltaic

Fluvial-deltaic	Contact area						Distance						Transition matrix					
	0	1	2	3	4	5	0	1	2	3	4	5	0	1	2	3	4	5
0	-	1.00	0.00	0.00	0.00	0.00	-	9.81	41.18	43.39	26.76	35.93	-	0.02	0.02	0.00	0.00	0.00
1	0.35	-	0.28	0.04	0.27	0.07	12.89	-	15.39	17.39	7.17	12.36	0.02	-	0.01	0.00	0.01	0.00
2	0.00	0.64	-	0.30	0.02	0.04	32.36	4.26	-	5.90	9.54	7.96	0.05	0.05	-	0.02	0.00	0.00
3	0.00	0.15	0.57	-	0.03	0.25	32.61	4.14	1.88	-	6.30	3.33	0.04	0.02	0.08	-	0.01	0.08
4	0.00	0.73	0.02	0.02	-	0.24	17.20	1.77	10.94	10.26	-	4.36	0.00	0.06	0.00	0.00	-	0.04
5	0.00	0.30	0.08	0.24	0.38	-	23.91	2.22	5.25	3.30	2.17	-	0.00	0.02	0.01	0.08	0.08	-

Figure 5.12 compares mean Δ MPHIST results of 5 realizations replicating TI2, from three types of lumping in hierarchical simulations. Results are then sorted in ascending order based on the 2×3×1 template. This TI has five categories; therefore it is applied with the same orderings as the 5-category 2D TI does in section 5.2.2. Standard MPS simulation shows higher Δ MPHIST results than hierarchical simulation.

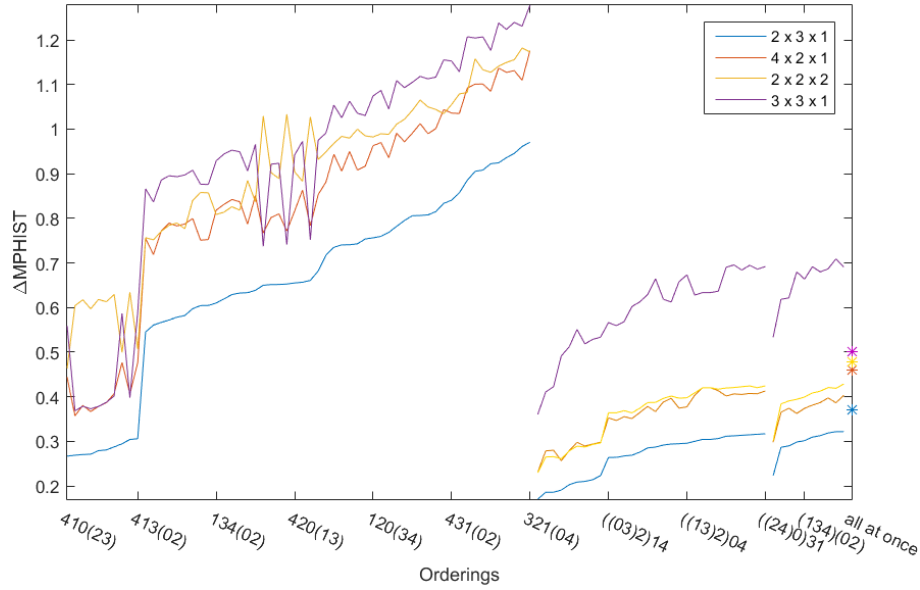


Figure 5.12: Comparing Δ MPHIST results for hierarchical simulation results to traditional simulation results

Table 5.13 compares the realizations from hierarchical simulation and standard simulation. The best ordering 410(23) in method #1, is simulating and freezing category 4 first, then 1 and finally 0, while category 2 and 3 are simulated last. Because category 4 is the least related to other categories, freezing 4 improves the simulation. The worst ordering is 321(04), which leaves category 0 and 4 separated and simulated together. According to Table 5.10, 0 is farthest from 4 and it cannot be transferred to 4; they should be merged not simulated. The worst ordering in method #2 combing 2 and 4 first, which indicates again that two far categories should not be simulated in the first step. The best ordering in third column is (234) (01), where 0 and 1 share the largest contact area, closest to each other, the greatest transition probability, and 1 is completely included in 0, hence they are combined.

Table 5.13: Comparing realizations of hierarchical simulation and traditional simulation

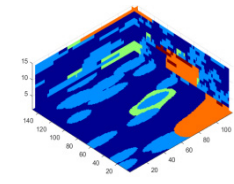
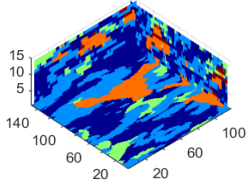
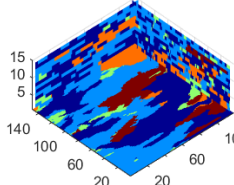
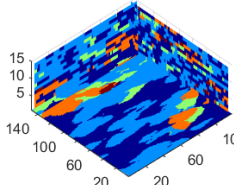
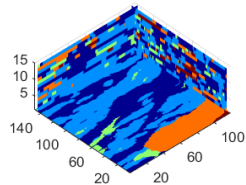
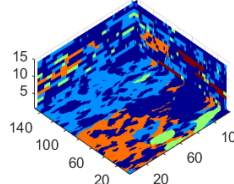
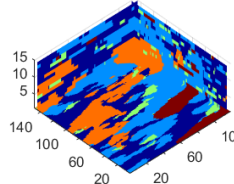
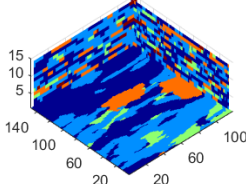
TI2		All at once [0.38]	
Min Δ MPHIST (temp size $2 \times 3 \times 1$)	Method #1 410(23) [0.27]	Method #2 ((02)1)43 [0.17]	Method #3 (01)(234) [0.23]
			
	321(04) [0.98]	((24)0)31 [0.33]	(23)(014) [0.32]
Max Δ MPHIST (temp size $2 \times 3 \times 1$)			

Figure 5.13 compares Δ MPHIST results of hierarchical and traditional simulation of TI3, and Table 5.14 shows different realizations. The best ordering for method #1 is 410(23), and the worst ordering is 321(04), both of which are consistent with the statistical relationships shown in Table 5.14, where 2 and 3 has highest transition probability that need to be simulated together, while 0 and 4 are not. In method #2, 0 and 4 are simulated in the first step and frozen for the rest of steps, which improves the stationarity of the TIs in rest of the steps. In method #3, 0 and 3 are ideal for merging, because 3 is contained in 0, while 0. Therefore, one category is contained in another should be merged rule is confirmed.

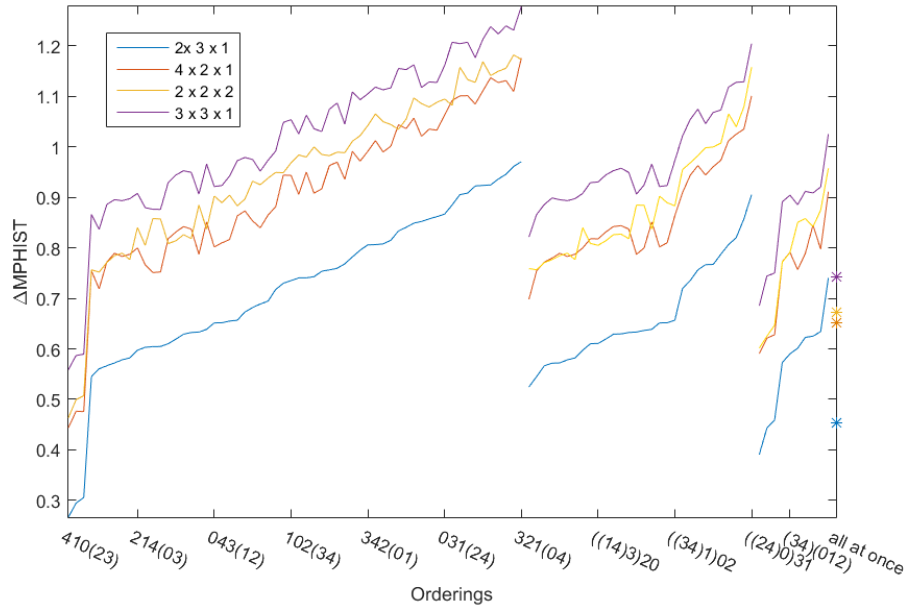


Figure 5.13: Comparing Δ MPHIST results for hierarchical simulation results to traditional simulation results

Table 5.14: Comparing realizations of hierarchical simulation and traditional simulation

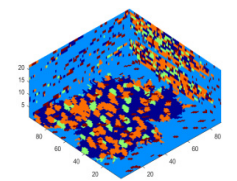
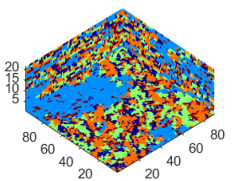
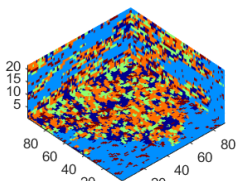
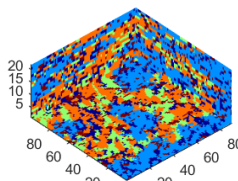
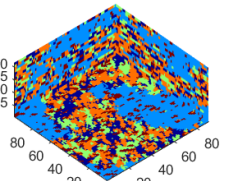
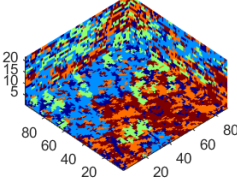
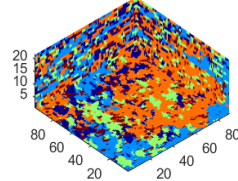
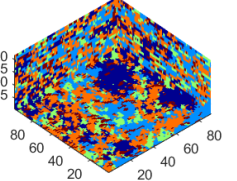
T13		All at once [0.45]	
Min Δ MPHIST (temp size $2 \times 3 \times 1$)	Method #1 410(23) [0.26]	Method #2 ((04)1)32 [0.52]	Method #3 (03)(124) [0.39]
			
Max Δ MPHIST (temp size $2 \times 3 \times 1$)	321(04) [0.95]	((24)0)31 [0.91]	(01)(234) [0.74]
			

Figure 5.14 compares results from the two-step method for TI4, which is merging two categories in the first step while others are simulated simultaneously. The best ordering occurs when combining 0 and 3 which conforms to the rule 3, merging the two least connected categories is good for hierarchical simulation; the second best ordering is merging 1 and 4 that shares largest contact area, which conforms to rule 1, merging two that are completely contact. The results of standard simulation are higher than hierarchical simulation.

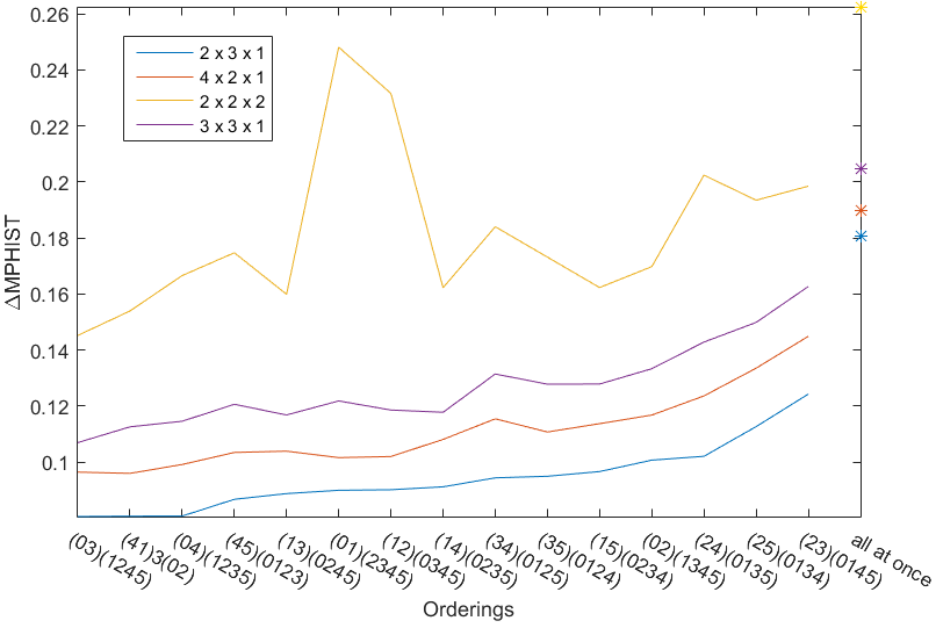
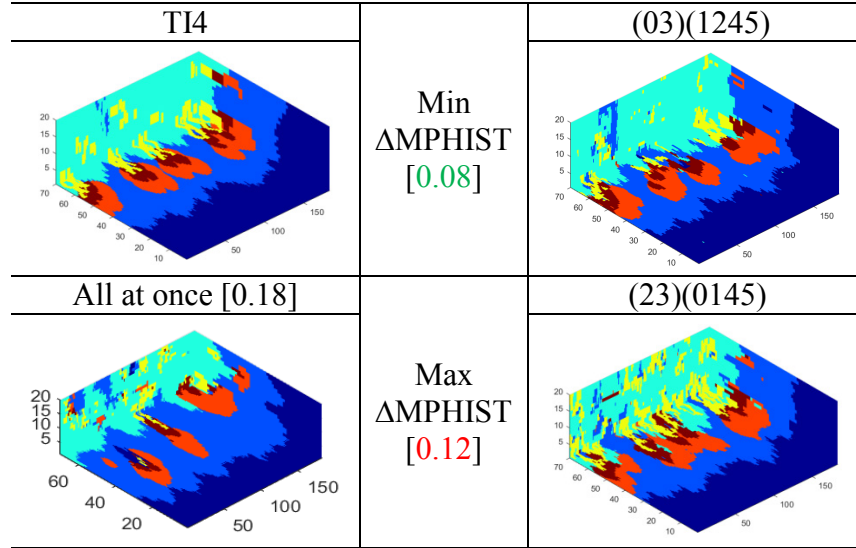


Figure 5.14: ΔMPHIST plot of the TI4

In Table 5.15, the worst ordering with Max ΔMPHIST show a little more messy feature reproductions than the ordering with Min ΔMPHIST, and it is still better than the standard simulation realization. The quality of the realizations also matches with the value of ΔMPHIST.

Table 5.15: Comparing realizations of hierarchical simulation and traditional simulation



5.5 Informed TI Patterns

In addition to the spatial relationship of categories, the number of informed pattern, are calculated to evaluate the stability of simulation results. TIs which include fewer informed patterns may be good for hierarchical method as they represent more repetitious of exiting patterns. Table 5.16 compares ideal ordering and informed patterns to the previous Δ MPHIST results. According to Table 5.16, all of the TIs of, except for the TI2, show great consistency between the number of informed patterns and previous metrics for assessing the quality of TI. They both have good results in Δ MPHIST test and informed pattern test. The only exception is applying the second lumping to TI2, the number of informed pattern does not match with the Δ MPHIST results, because it is a complex lumping method that results in more uncertainty. Overall, using the number of informed patterns is convincing to predict an appropriate ordering in hierarchical simulation.

Table 5.16: Comparing the best ordering in informed patterns method to Δ MPHIST results; the value in fourth column is the location of the best ordering found in “# of informed

patterns” test in Δ MPHIST test

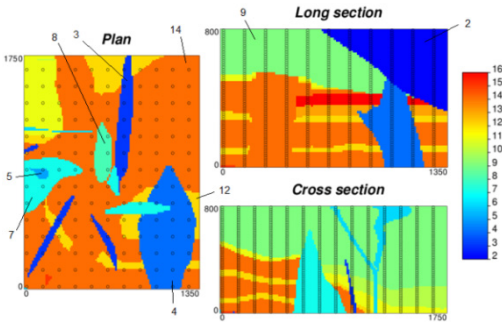
TI	The order of lumping type	The best ordering (by informed pattern)	Δ MPHIST results	# of total lumpings
ice-edge	1	3,12	1	3
Walker lake	1	1,23	1	3
crystal	1	1,23	2	3
marble	1	1,23	2	3
5-category	1	5,4,1,(23)	5	60
	2	((45)1) 23	7	30
	3	(24), (135)	5	10
TI2	1	4,3,2,(01)	36	60
TI2	2	((34)1)02	25	30
	3	(01)(234)	1	10
TI3	1	4,1,2,(03)	2	60
	2	((12)3)04	12	30
	3	(03)(124)	1	10
TI4	2	(14),(0235)	2	15
porphyry	1	4,1,2 3	6	12
	2	(14),2,3	1	6

5.6 The Large Copper TI Example

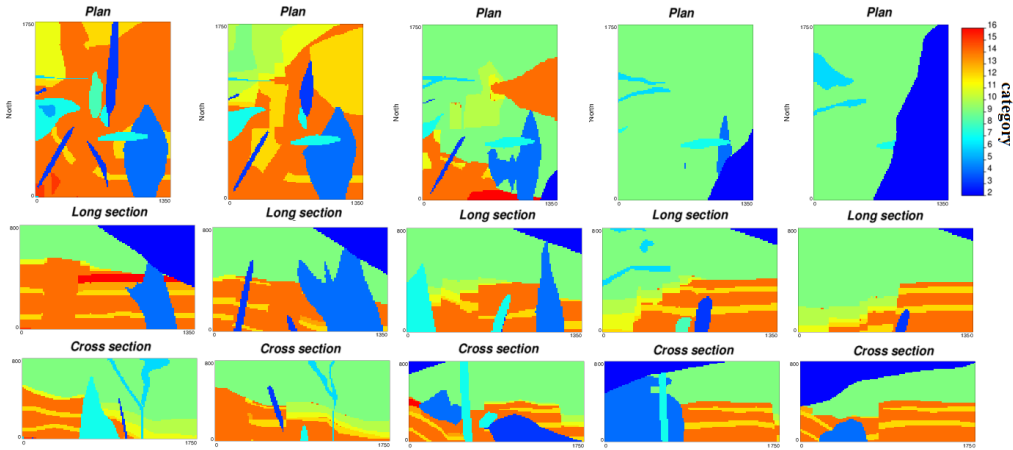
Background on the large copper TI was introduced in Chapter 4, and standard MPS simulation was applied with poor results, because of the large number of categories and resulting a few cells. Therefore, hierarchical simulation is applied with consideration given to known geological ordering. According to the rules summarized previously, the relationship between categories helps decide the optimal ordering. Geological movement influences on the formation of the rock, which is reflected in the relationships between

categories. Figure 5.15 illustrates the relationship between categories in the TI. The workflow of lumping categories in hierarchical simulation is:

1. Faulted blocks (categories 2, 9, and 14) and categories (5, 6, 8, 12, and 15) which are contained in the faulted blocks and have small proportions and merged first, since they comprise the background and share a large contact area.
2. The combination in the first step is reversed that 2, 9, 14 and other 5 categories are separated, re-coded into 1, 2, 3, and 4 while the rest 7 categories are lumped as 0 and will not be separated again.
3. Lumping separated intrusions/breccias (5, 6, 8, 12 and 15).
4. Lumping faulted blocks (2, 9 and 14).
5. Re-combing the final results.



(a)



(b)

Figure 5.15: Slices of the TI: (a) the locations of some of the categories and wells; (b) show five slices in three sections, which will be compared to the realizations

Realizations of hierarchical simulation are shown in Figure 5.16, and they better replicate most features and details from the original TI when compared to traditional simulation (Figure 5.17). Comparing to standard simulation realizations presented in Figure 5.17, which is conditioned to 20×20 drillings, but still reproduces fewer features from the TI than hierarchical realizations. Because the number of categories decreased and the original TI is simplified, hierarchical simulation has a clear advantage when using this complex TI.

The Δ MPHIST results of hierarchical simulation and standard simulation are shown in the corresponding figure captions, which are based on the template size 2×2 and 2×3 . The Δ MPHIST results of hierarchical realization are much lower than the values of standard realization, which matches with the visual outcomes.

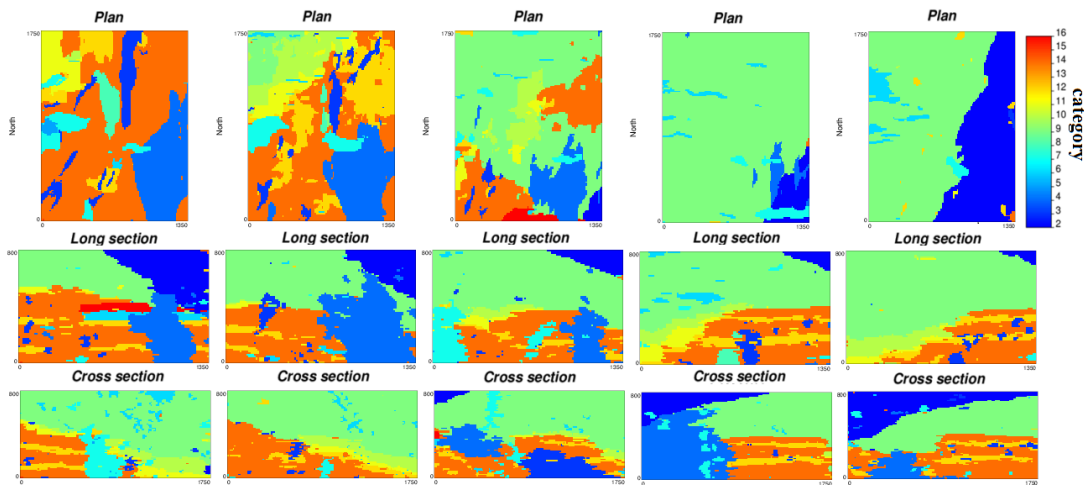


Figure 5.16: Six slices of hierarchical simulation (Δ MPHIST: 2×2 [0.11], 2×3 [0.14])

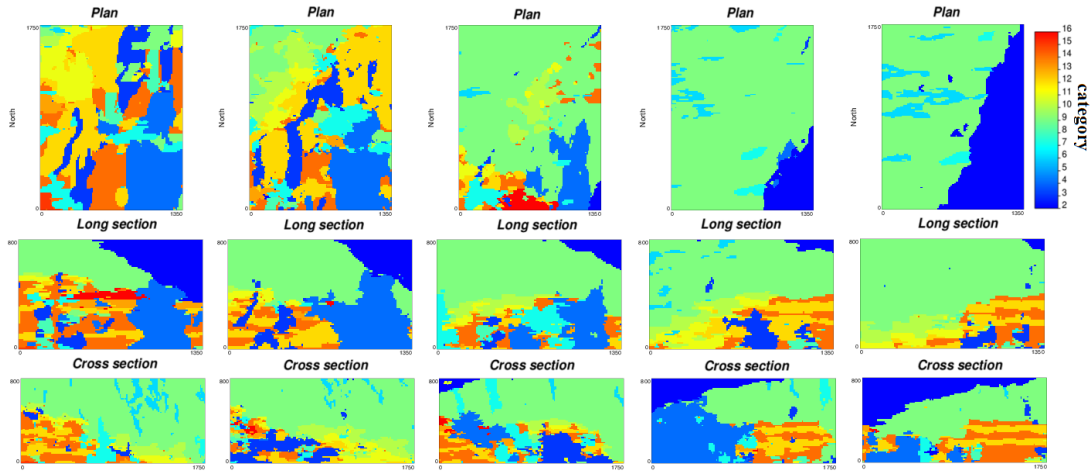


Figure 5.17: Realizations of standard MPS simulation (Δ MPHIST: 2×2 [0.33], 2×3 [0.35])

5.7 Discussion

Though TIs with more than three categories are proved to be secondarily to poorly stationary, the implementation of combing categories changes the formation of the TI and may change quality of the TI. Rules are generated through numerous hierarchical simulations on many TIs:

1. Categories that share large contact areas should be considered as a group. If one is contained in another category, they can be merged in first steps; or if they are not similar, they should be simulated together in the last step.
2. From the example of 5-category TI, the most isolated category should be simulated at first. Therefore it will be frozen for the rest of the steps.
3. From the examples in section 5.3.1 that categories share few connections need to be merged to improve the quality of the TI.
4. Categorical relationships do help predict what type of lumping works for the TI.
5. TIs that comprise of fewer informed patterns with more repetitive features that are ideal for hierarchical simulation.

Geological background directly effects the formation of the TI, and categorical relationships are reflected through statistics. Visual comparison is important as well as the statistical results. Testing the statistical relationship is fast and straightforward, and the quality of the realizations reflects that using categorical relationships to predict lumping is convincing as well.

Chapter 6

Conclusions

6.1 Research Conclusions and Contributions

MPS modeling has been widely developed and applied to numerous fields of geological research. MPS simulation depends on a conceptual geological model in the form of a TI, which is a numerical representation of geological heterogeneity relevant for the modeling domain. SNESIM, one of the commonly used MPS algorithms was implemented and all inputs analyzed to provide guidance to practitioners wanting to obtain optimal pattern reproduction through MPS simulation. The following content are the key contributions of this work.

The first contribution is assessing the stationarity of the TI, which assess whether the TI has repeated features thus making it acceptable for use in MPS simulation. There are several issues encountered when using a “non-stationary” TI in MPS simulation: (1) a non-stationary TI cannot represent the features in the full domain of the researching area; (2) the quality of realizations is usually poor, because the probability of finding the MPS pattern from a realization is extremely low resulting in poor reproduction of the TI features. Stationarity was quantified through four methods including: distribution of categories, MPHIST and Euclidean distance; and through oriental distribution, which is defined by “normality”, “uniformity” and “repeatability”. The statistical tests in Chapter 2 showed that the TIs are either “stationary”, “medium” or “non-stationary”, while some are uncertain and their quality cannot be predicted until they are implemented in unconditional. It was found that TIs that scored higher on these stationarity metrics generated realizations that better

reproduce the features in the TIs. Cut offs were selected to determine the stationarity level of a TI for prediction of realization quality. Since the quality of a TI has large influence on the quality of the realizations, it is not trivial to assess the stationarity.

The second contribution is selecting optimal input parameters for MPS simulation to improve feature reproduction in realizations. Many realizations were generated for different parameter settings and compared to determine optimal settings. Δ MPHIST was found to be a good judge of realization quality. The analysis of realizations indicates that there are optimal parameters setting, which including: using 40-60 data for 2D simulation; using 50 or more data for 3D simulation; using a square template shape or using a shape similar to the dominant object in the TI for elongated features; using 4-5 multi grids; using a search radii proportional to the dominant object in the TI; and finally using an experimental value, such as 16, of “maximum of conditioning data” is certainly alright since it makes little differences on results.

Finally, the second contribution is applying a hierarchical approach in MPS simulation. The simultaneous implementation of MPS simulation is difficult to apply to a TI with large number of categories, as the difficulty of exact replicates increases. The hierarchical methodology is employed to improve the accuracy of TI feature reproductions. Therefore, the third contribution is determining a reasonable way to lump categories in a TI that is appropriate for hierarchical simulation approach. Having reasonable order is important for feature reproduction and rules are presented to help determine which categories to merge:

1. Categories that share large contact areas should always be considered together. If one is contained in another category, they can be merged; or if they are not similar, they should be simulated together in the last step.

2. The most isolated category should be simulated at first; therefore it is frozen for the rest of the steps and enhances the replication of features. From the perspective of repeatability, separating the category with unique shape will improve the stationarity of TI, which improves the results as well.
3. Categories that share a few connections need to be merged to improve the quality of the TI.

6.2 Recommendations

Various types of TIs are used with MPS simulation in this thesis. The suggestions provided here will help predict how a given TI will perform and aids practitioners understand of their models and results; selecting an optimal setting for SNESIM and judging the realizations helps improve better realizations in MPS simulation, and applying hierarchical rules for a complex TI can encourage implementation of MPS modeling on various geological models.

Bibliography

- Arpat, G. B. (2005). *Sequential Simulation with Patterns*. Stanford University.
- Boisvert, J. B., Pyrcz, M. J., & Deutsch, C. V. (2007). Multiple-Point Statistics for Training Image Selection. *Natural Resources Research*, 313–321.
- Boisvert, J. B., Pyrcz, M. J., & Deutsch, C. V. (2006). *Choosing Training Images and Checking Realizations with Multiple Point Statistics*. Centre for Computational Geostatistics Annual Report.
- Caers, J. (2002). Geostatistical History Matching Under Training-Image Based Geological Model Constraints. *SPE* (pp. 115-135). San Antonio: Society of Petroleum Engineers.
- Caers, J., & Arpat, G. B. (2007). Conditional simulation with patterns. *MATHEMATICAL GEOLOGY*, 177-203.
- Comunian, A., Renard, P., & Julien, S. (2011). 3D multiple-point statistics simulation using 2D training images. *Computers & Geosciences*, 49-65.
- Deutsch, C. V. (1992). *Annealing Techniques Applied to Reservoir Modeling and the Integration of Geological and Engineering (Well Test) Data*. Stanford, CA: Stanford University.
- Deutsch, C. V., & Pyrcz, M. J. (2014). *Geostatistics Reservoir Modeling*. Oxford University Press.
- Goodfellow, R., Consuegra, F. A., Dimitrakopoulos, R., & Lloyd, T. (2012). Quantifying Multi-Element and Volumetric Uncertainty, Coleman McCreech Deposit, Ontario, Canada. *Computers & Geosciences*, 71–78.
- Guardiano, F. B., & Srivastava, R. M. (1993). Multivariate Geostatistics: Beyond Bivariate Moments. In *Geostatistics Tróia '92* (pp. 133-144).
- Hashemi, S., Javaherian, A., Ataee-pour, M., & Khoshdel, H. (2014). Two-point versus multiple-point geostatistics: the ability of geostatistical methods to capture complex geobodies and their facies associations—an application to a channelized carbonate reservoir, southwest Iran. *Journal of Geophysics and Engineering*, 65002-65016.
- Liu, Y. (2006). Using the SNESIM Program for Multiple-Point Statistical Simulation. *Computers & Geosciences*, 1544–1563.
- Lyster, S., & Deutsch, C. V. (2006). *Short Note: An Entropy-Based Approach to Establish MPS Templates*. Centre For Computational Geostatistics.
- Lyster, S., Oy, L., & Clayton, D. V. (2004). Simulated Annealing Post Processing for Multiple Point. *CCG Annual Report 06*. University of Alberta: Centre for Computational Geostatistics.

- Maharaja, A. (2004). *Hierarchical Simulation of Multiple-Facies Reservoir Using Multiple-Point Statistics*. Stanford University (pp. 13-29).
- Mariethoz, G., & Caers, J. (2014). *Training Image Library*. Retrieved from Multiple-point Geostatistics: Stochastic Modeling with Training Images: <http://www.trainingimages.org/training-images-library.html>
- Matheron, G. (1962). *Traité de géostatistique appliquée*. Paris: Editions Technip.
- Meerschman, E., Van Meirvenne, M., Van De Vijver, E., & Saey, T. (2013). Mapping complex soil patterns with multiple-point geostatistics. *European Journal of Soil Science*, 183-191.
- Mirowski, P. W., Tetzlaff, D. M., Davies, R. C., McCormick, D. S., Williams, N., & Signer, C. (2009). Stationarity Scores on Training Images for Multipoint Geostatistics. *Mathematical Geosciences*, 447-474.
- Mood, A. M. (1940). The Annals of Mathematical Statistics. *Mathematical Statistics*, 367--392.
- Norrena, P. K. (2007). *Decision Making Using Geostatistical Modeling of Uncertainty*. Edmonton: University of Alberta.
- Pyrz, M. J., Boisvert, J. B., & Deutsch, C. V. (2008). A Library of Training Images for Fluvial and Deepwater Reservoirs and Associated Code. *Computers & Geosciences*, 542-560.
- Renard, P., & Mariethoz, G. (2014). Special Issue on 20 Years of Multiple-Point Statistics: Part 1. *Mathematical Geosciences*, 129-131.
- Rezaee, H., Asghari, O., Koneshloo, M., & Ortiz, J. M. (2014). Multiple-point geostatistical simulation of dykes: application at Sungun porphyry copper system, Iran. *Stochastic Environmental Research and Risk Assessment*, 1913-1927.
- S. Strebelle, C. C. (2014). Solving Speed and Memory Issues in Multiple-Point Statistics Simulation Program SNESIM. *Mathematical Geosciences*, 171-186.
- Scheidt, C., & Caers, J. (2007). *A Workflow for Spatial Uncertainty Quantification using*. Stanford University: SCRF report 20.
- Sebastien, S., & Zhang, T. (2004). NON-STATIONARY MULTIPLE-POINT GEOSTATISTICAL MODELS. In O. D. Leuangthong, *Geostatistics Banff* (pp. 235-244).
- Silva, D. (2014). *Guide to MPS Simulation with SNESIM Algorithm*. University of Alberta: Centre for Computational Geostatistics.
- Silva, D., & Deutsch, C. V. (2014). *Thoughts on the Stationarity of Training Images*. Edmonton: CCG Annual Report.
- Straubhaar, J., Walgenwitz, A., & Renard, P. (2014). Parallel Multiple-Point Statistics Algorithm Based on List and Tree Structures. *Mathematical Geosciences*, 131-147.

- Strebelle, S. (2002). Conditional Simulation of Multiple Point Statistics. *Mathematical Geology*, 1–21.
- Strebelle, S., & Cavelius, C. (2014). Solving Speed and Memory Issues in Multiple-Point Statistics Simulation Program SNESIM. *Mathematical Geosciences*, 171–186.
- Suzuki, S., & Caers, J. (2006). History Matching with an Uncertain Geological Scenario. *SPE Annual Technical Conference and Exhibition* (pp. 24-27). San Antonio: Society of Petroleum Engineers.
- Tan, X., Tahmasebi, P., & Caers, J. (2014). Comparing Training-Image Based Algorithms Using an Analysis of Distance. *MATHEMATICAL GEOSCIENCES*, 149-169.
- University of Southern California, (2013, September 16th). Retrieved from Spatial Statistics PM 599: <http://www-hsc.usc.edu/~mereditf/Spatial%20Statistics%203.pdf>
- Zhang, T. (2006). *Filter-Based Training Pattern Classification for Spatial Pattern Simulation*. Stanford University.
- Zhang, T., Pedersen, S. I., & Knud, C. (2012). Memory-Efficient Categorical Multi-point Statistics Algorithms Based on Compact Search Trees. *Mathematical geosciences*, 863–879.

Appendix A – Software

A.1 Introduction

Three GSLIB style software programs have been updated and developed to support the research presented in this thesis. The update of the original SNESIM program is based on the work of Strebelle (2000), and the development of two programs DISTANCE and CONTACT AREA introduced in section 7.2, thanks to the guidance of Boisvert. This appendix provides a description of the purpose and parameters details for the programs that support hierarchical simulation.

A.2 Updated SNESIM Program

To freeze one of the simulated categories at the following steps in hierarchical simulation, one line was added to the original SNESIM program, which is located in row 11 “nosim.out”. This is a binary file that contains the information to skip the location of code “0” and keep simulating on the location of code “1”. The “nosim” file is the same size as the TI and it is obtained from the realization in the previous simulation.

As “0” is neglected at the second or following step of simulation, the proportions of categories are changed as well. The proportion of the category i being simulated is computed by:

$$\Pr(i)' = \frac{\Pr(i)}{1 - \Pr(0)} \quad \text{Equation A.1}$$

Where \Pr represent the proportion, $\Pr(i)'$ stands for the new proportion of the category i than the original proportion in the TI. The details of parameters are given as follow:

```

Parameters for SNESIM
*****
1   START OF PARAMETERS:
2   data.dat                - file with original data
3   1 2 3 4                - columns for x, y, z, variable
4   3                      - number of categories
5   0 1 2                  - category codes
6   0 0.4 0.6              - (target) global pdf
7   0                      - use (target) vertical proportions
(0=no, 1=yes)
8   vertprop.dat           - file with target vertical
proportions
9   1 0.5                  - target pdf repro. (0=no, 1=yes),
parameter
10  0                      - debugging level: 0,1,2,3
11  nosim.out              - indicates where to sim (same size
as nx, ny, nz), 0=no sim, 1=sim, hard coded to be in col 1
12  snesim.dbg             - debugging file
13  snesim2.out            - file for simulation output
14  1                      - number of realizations to generate
15  100 0.5 1.0            - nx,xmn,xsiz
16  100 0.5 1.0            - ny,ymn,ysiz
17  1 0.5 1.0              - nz,zmn,zsiz
18  69069                  - random number seed
19  template.dat           - file for primary data template
20  16                     - max number of conditioning primary
data
21  0                      - max number of data per octant
22  16                     - min number of data events
23  1 0                    - number of mult-grids, number with
search trees
24  p2.dat                 - file for training image
25  100 100 1              - training image dimensions: nxtr,
nytr, nztr
26  1                      - column for training variable
27  100.0 100.0 1.0        - maximum search radii
(hmax,hmin,vert)
28  0.0 0.0 0.0           - angles for search ellipsoid
29  -remove data from the original data file where you do not want to
simulate (according to the nosim.out file)

```

A.3 Created Statistical Relationship Calculation Program

A.3.1 Distance

It has been indicated in Chapter 5 that statistical relationship can help predict lumpings that can generate better realizations in hierarchical simulation. The first program is computing the distance between two categories. The final result will be presented as a $K \times K$ matrix, where K is the number of categories.

```

Parameter for Distance
*****

1  START OF PARAMETERS:
2  train.dat           -input file with categorical variable
3  1                   -column for the input
4  100 0.5 1.0        -nx, xmin, xsize
5  100 0.5 1.0        -ny, ymin, ysize
6  1 0.5 1.0          -nz, zmin, zsize
7  5                   -number of categories
8  1 2 3 4 5          -first plot file
9  distance.out        -file for output matrices

```

A.3.2 Contact Area

The second program is computing the contact area between two categories. The final result will be presented as a $K \times K$ matrix, where K is the number of categories.

```

Parameters for Contact Area
*****

1  START OF PARAMETERS:
2  train.dat           -input file with categorical variable
3  1                   -column for the input
4  100 0.5 1.0        -nx, xmin, xsize
5  100 0.5 1.0        -ny, ymin, ysize
6  1 0.5 1.0          -nz, zmin, zsize
7  5                   -number of categories
8  1 2 3 4 5          -first plot file
9  contact.out        -file for output matrices

```

Appendix B – Workflow for Lumping in

Hierarchical Approach

Hierarchical simulation has been discussed in Chapter 5. The purpose is to recode the original TI to another TI with different category combinations, in order to generate better realizations than standard MPS simulation. There are three types of lumping implemented in this thesis when a TI has more than three categories. The workflow of three types of lumping and the recombination of the final realizations are given following:

- 1.1) Consider a TI with five categories 1, 2, 3, 4 and 5. The first lumping is to recode the original TI into a binary TI as shown in Figure B.1. Specifically, four categories are merged as “1” and the other category is changed to “0”.

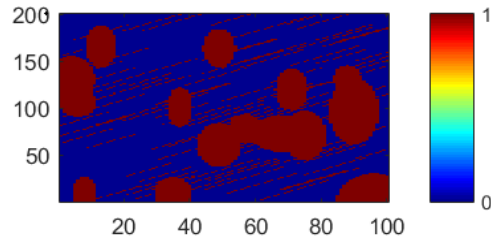


Figure B.1: The binary TI in the first step

- 1.2) The TI in the first step is re-coded: “0” is kept and is frozen in simulation; one of the categories from “1” is separated to “2”. There are 3 categories in total.

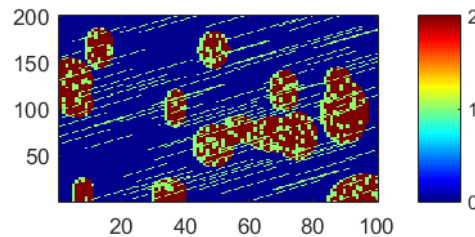


Figure B.2: The TI in the second step

- 1.3) “2” in the second step is re-coded to “0” and is frozen in this step of simulation. Another category from “1” is separated to “2”.

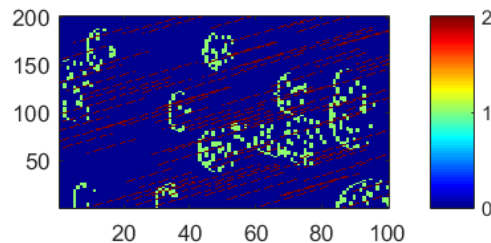


Figure B.3: The TI in the third step

- 1.4) In this step, only two categories are left as “1”, one of the categories can be re-coded to “2”, while others are unchanged. Three categories are “0” and frozen in this step.

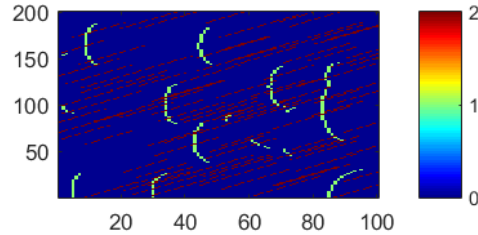


Figure B.4: The TI in the fourth step

- 2.1) The second type of lumping is to merge three categories as “0”, leaving other two as “1” and “2”.

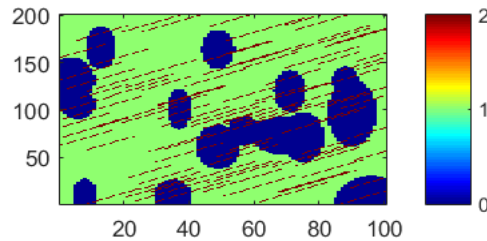


Figure B.5: The TI in the first step

- 2.2) The combination in the first step is reversed: three “0” is re-coded to “1”, “2”, and “3”, while other two is merged as “0” and frozen in simulation.

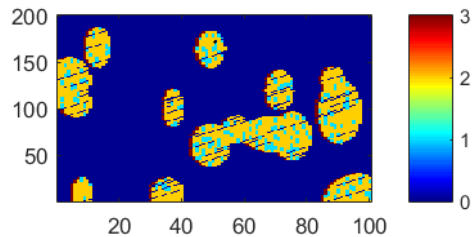


Figure B.6: The TI in the second step

- 2.3) “1” in the second step is merged into “0”, changing other two categories into “1”, and “2”.

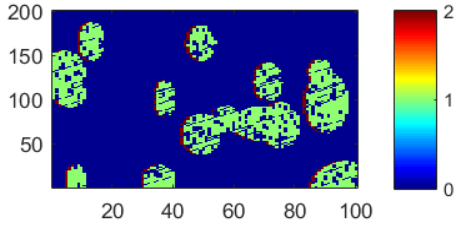


Figure B.7: The TI in the third step

- 3.1) The third type of lumping is the easiest: combing two categories while leaving other three categories into “1”, “2”, and “3”.

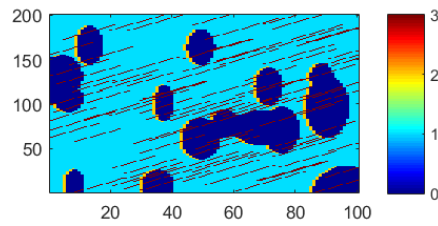


Figure B.8: The TI in the first step

- 3.2) The combination in the first step is reversed: two “0” are divided into “1” and “2”, and other three separated categories are merged together as “0”.

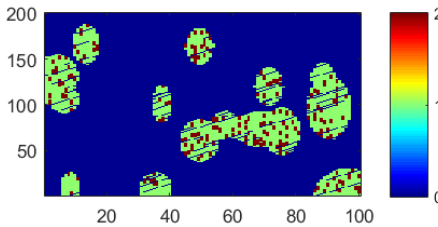


Figure B.9: The TI in the second step

Final results are cookie-cut together, and the corresponding categories are re-coded to their original status, same as the TI. Figure B.10 is the demonstration of cookie-cutting the realizations from the second lumping, and re-coding it to the final realization.

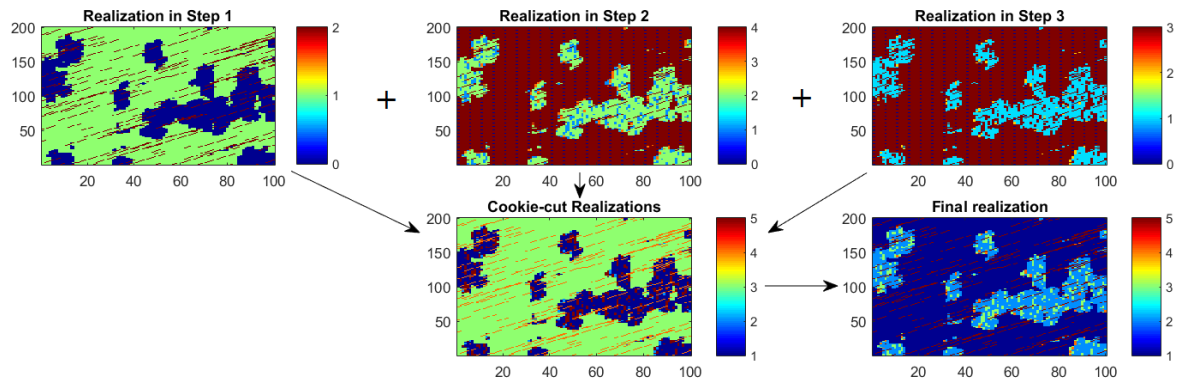


Figure B.10: The demonstration of cookie-cut realizations and re-coding to final realization